DESIGN OF BIDIRECTIONAL DC-DC CONVERTER FOR FUEL CELL BASED ELECTRIC VEHICLE

A PROJECT REPORT

Submitted by

BARATH NARAYANAN A	**715517105005**
SHREYAS S	**715517105037**
SUBHASH SADACHARAM	**715517105047**
PAUL ANAND S	**715517105059**

In partial fulfillment for the award of the degree

Of

BACHELOR OF ENGINEERING

IN

ELECTRICAL AND ELECTRONICS ENGINEERING

PSG INSTITUTE OF TECHNOLOGY AND APPLIED RESEARCH,

COIMBATORE

ANNA UNIVERSITY: CHENNAI 600025

APRIL 2021

ANNA UNIVERSITY: CHENNAI 600025

BONAFIDE CERTIFICATE

Certified that this project report " **DESIGN OF BIDIRECTIONAL DC-DC CONVERTOR FOR FUEL CELL BASED ELECTRIC VEHICLE** " is the bonafide work of " **BARATH NARAYANAN A , SHREYAS S , SUBHASH SADACHARAM , PAUL ANAND S** " who carried out the project work under my supervision .

SIGNATURE
Dr. C L Vasu
HEAD OF THE DEPARTMENT
Professor & HoD
Department of Electrical and Electronics Engineering
PSG Institute of Technology and Applied Research

SIGNATURE
Dr. C S Subash Kumar
SUPERVISOR
Associate Professor
Department of Electrical and Electronics Engineering
PSG Institute of Technology and Applied Research

Certified the candidate was examined in the viva-voce examination held on_____.

Internal examiner **External examiner**

ABSTRACT

In recent years, the application of bidirectional DC-DC converters has increased in fuel cell operated electric vehicles and battery-based energy storage systems. The rapid advances in automotive technology and power electronics have enabled the significant development in fuel cell based electric vehicles. The main advantages of fuel cells are green power generation, high density current output and higher efficiency of operation. Still, fuel cell has limitation with respect to massive energy storage capability. Hence in electric vehicle applications, an auxiliary energy storage device (i.e., lithium-ion battery) is used in this project. A bidirectional DC-DC converter is necessary between the energy storage battery and the fuel cell supply to match the required voltage level. In this project a complete design of fuel cell electric vehicle along with converters and control strategy that catalyses the stable power generation process is studied and analyzed using MATLAB SIMULINK.

ACKNOWLEDGEMENT

We would like to express our gratitude to **Dr. G Chandramohan**, **Principal**, **Dr. P V Mohanram, Secretary**, and the management of PSG Institute of Technology and Applied Research , for providing us the opportunity to carry out our project with the best infrastructure and facilities .

We extend our sincere thanks to **Dr. C L Vasu**, Professor and Head of the Department of Electrical and Electronics Engineering for providing consistent support through the project .

We extend our sincere thanks to **Dr. C S Subash Kumar**, Associate Professor, our project guide, **Mr. S Ravikrishna**, Assistant Professor (Sr. Gr.) , and **Mr. M Sathyanathan** , Assistant Professor (Sr.Gr.), Department of Electrical and Electronics Engineering for giving their unfailing support throughout the project .

We extend our gratitude to all the faculty and staff members, friends and our parents for their constant support and guidance .

TABLE OF CONTENTS

LIST OF TABLES

LIST OF FIGURES

LIST OF ABBREVIATIONS

FCEV	-	Fuel Cell Electric Vehicle
EV	-	Electric Vehicle
HEV	-	Hybrid Electric Vehicle
BMS	-	Battery Management System
DC	-	Direct Current
CCM	-	Continuous Conduction Mode
IC	-	Internal Combustion
BLDC	-	Brushless Direct Current
Ph	-	Phase
Li	-	Lithium
PEM	-	Proton Exchange Membrane
MATLAB	-	Matrix Laboratory
P	-	Proportional
PI	-	Proportional Integral
PID	-	Proportional Integral Derivative
IBDC	-	Isolated Bidirectional DC-DC converter
NIBDC	-	Non-Isolated Bidirectional DC-DC converter
SoC	-	State of Charge
OCV	-	Open Circuit Voltage

Hp	-	Horsepower
EMF	-	Electromotive Force
FIS	-	Fuzzy Inference System
ANN	-	Artificial Neural Networks
MPC	-	Model Predictive Control
IC	-	Integrated Circuits
C	-	Coulomb

CHAPTER 1

INTRODUCTION

1 INTRODUCTION

Improper energy utilization, reduced performance, optimum range are the challenges faced in the design of Electric Vehicles (EV) and Hybrid Electric Vehicles (HEV). This has led to the exploration in the field of Battery Management Systems (BMS) and automotive electronics which look to overcome the present hurdles. In this regard, Bidirectional DC-DC convertors have been employed in HEV and Fuel Cell Electric Vehicles (FCEV). As the current in Bidirectional DC-DC convertors can change direction from source to load or vice versa, power can be transferred between two DC sources without any change in the polarity of the convertor. This topology allows the convertor to operate in the Continuous Conduction Mode (CCM). The output voltage can be controlled with or without the load .

1.1 THE NEED FOR FCEVs

Environmental degradation due to fuel emissions from IC engine vehicles has effectively lowered the air quality standards below the permissible limits. In addition to this, the fuel we use today to power in our automobiles is heading to exhaustion. In order to resolve this crisis, EVs were introduced.

With minimal environmental pollution, zero emissions and enhanced efficiency, the EVs pave the way for clean and green energy utilization. By

substituting the IC engine with motors, greater tractive effort can be generated. Batteries, fuel cells provide a great alternative to conventional energy sources as they can be recharged and reused. The optimum power flow in the system is facilitated by using power electronic convertors and its control algorithms .

1.2 CONCEPT OF FCEVs

The basic system consists of

- Two alternative energy sources
- A DC-DC convertor
- A power distribution system
- 3-ph Inverter
- BLDC Motor

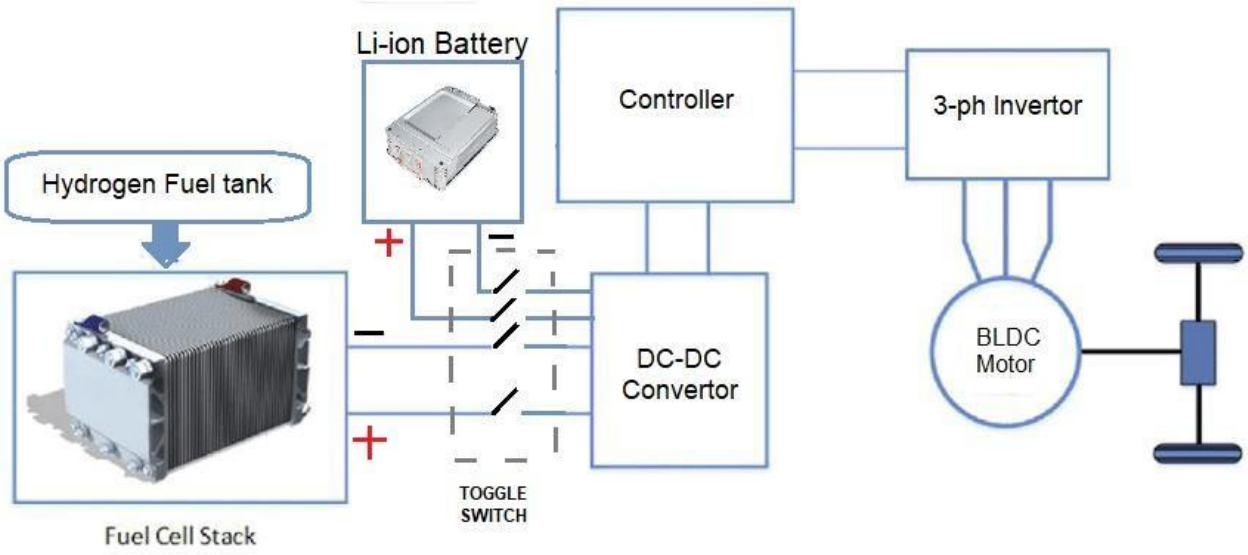

Fig. 1.1 Block diagram of Proposed Fuel Cell Electric Vehicle

The DC-DC convertor facilitates the usage of alternate power sources to drive the BLDC motor. A fuel cell equipped with a hydrogen fuel tank is utilized. Also, the actions of regenerative braking and forward motoring can be realized using this sub-system. The above system shown in Fig. 1.1 provides a technique to control the dynamic load conditions with the help of a controller [19].

1.3 SOURCES USED IN FCEVs

A power source is required to drive the proposed electrical system, namely two power supplies are discussed as follows.

1.3.1 Li-ion BATTERY

A lithium-ion (Li-ion) battery is an advanced battery technology that uses lithium ions as a key component of its electrochemistry. During a discharge cycle, lithium atoms in the anode are ionized and separated from their electrons. The lithium ions move from the anode and pass through the electrolyte until they reach the cathode, where they recombine with their electrons and electrically neutralize. The lithium ions are small enough to be able to move through a micro-permeable separator between the anode and cathode. In-Spite of lithium's small size, Li-ion batteries are capable of having a very high voltage and charge storage per unit mass and unit volume. Lithium ion batteries provide improved levels of capacity combined with reliable operation when compared to other forms of cell [3].

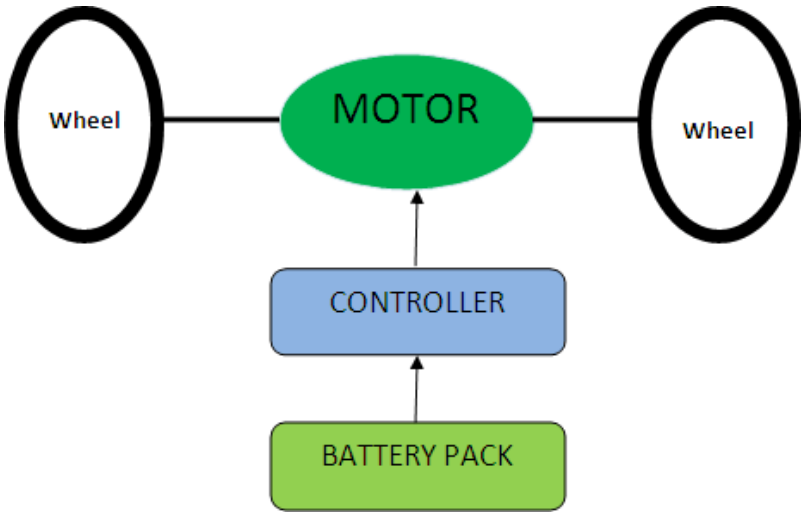

Fig. 1.2 Flow diagram of Battery Powered Electric Vehicle

As a result of their characteristics, Lithium Ion, or Li-ion batteries have become the battery technology of choice in a variety of areas. Li-ion batteries are used almost exclusively in mobile phones, laptops, electric vehicle propulsion and many other electronic gadgets. Fig. 1.2 shows the flow diagram of a battery powered Electric Vehicle.

1.3.2 FUEL CELL

The most common type of fuel cell for vehicle applications is the polymer electrolyte membrane (PEM) fuel cell. In a PEM fuel cell, an electrolyte membrane is sandwiched between a positive electrode (anode) and a negative electrode (cathode). Hydrogen is introduced to the anode, and oxygen (from air) is introduced to the cathode. The hydrogen molecules break apart into protons and electrons due to an electrochemical reaction in the fuel cell catalyst. Protons then travel through the membrane to the cathode [9] .

The electrons are forced to travel through an external circuit to perform work (providing power to the electric car) then recombine with the protons on the cathode side, where the protons, electrons, and oxygen molecules combine to form water. Fig. 1.3 shows the flow diagram of a generic fuel cell electric vehicle .

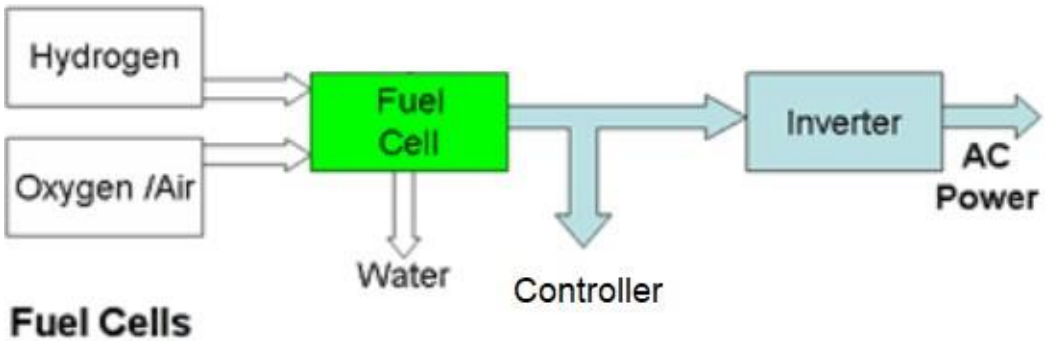

Fig. 1.3 Flow diagram of a Generic Fuel Cell Electric Vehicle

1.4 POWER ELECTRONIC CONVERTER

Practical electronic convertors employ techniques for switching. Switched mode DC-to-DC converters convert one level of DC voltage to another, which may be greater or lesser, by temporarily storing the input power and releasing that energy to an output at a different voltage. The storage may be either in components of magnetic field storage (inductors, transformers) or in components of electric field storage (capacitors) [12]. This stepping up (boost) and stepping down of voltage (buck) is achieved through soft - switching technique which is highly efficient . Though continuous usage requires complex control strategies and specialized semiconductor devices, these converters are the backbone in the field of automotive

electronics. Most DC-DC converters are designed to allow power flow from input to output in only one direction . However, by replacing all diodes with independently controlled active rectification all switching regulator topologies can be made bidirectional and be able to move power in either direction . For example, a bidirectional convertor is useful in applications requiring regenerative braking. Though requiring a few components, switching converters are electronically complex. Their cost in voltage dropping application is higher than linear regulators, but their cost has shrunk with advances in chip design. Available as Integrated-Circuits (ICs), DC-to-DC converters require few additional components. Converters are also available as full, ready-to-use hybrid circuit modules within an electronic assembly [20] .

The various type of converters used here as follows :

1. Buck Converter
2. Boost Converter
3. Buck-Boost Converter
4. Bidirectional Converter

1.4.1 BUCK CONVERTER

It is also known as a step-down converter. It decreases its output voltage from its input voltage while increasing output current from its input current.

$$V_{in} > V_{out} \text{ and } I_{in} < I_{out}$$

1.4.2 BOOST CONVERTER

It is also known as a step-up converter . It increases output voltage from its input voltage while decreasing output current from its input current .

$V_{in} < V_{out}$ and $I_{in} > I_{out}$

1.4.3 BUCK-BOOST CONVERTER

It is also known as the step-up and step-down transformers . The output Voltage of the DC-DC convertor is less than input voltage when it operates in buck mode or greater than the input voltage when it operates in the boost mode. The magnitude of the output voltage depends on the duty cycle. By Using the low conversion energy, the input power is equal to the output power .

Input Power (P_{in}) = Output Power(P_{out})

1.4.4 BIDIRECTIONAL CONVERTER

There are basically two types of Bidirectional DC-DC converter based on the galvanic isolation provided between input and output .

- Non - Isolated Bidirectional DC-DC Converter (NIBDC)
- Isolated Bidirectional DC-DC Converter (IBDC)

1.4.4.1 NIBDC

NIBDC is a converter which does not use a high frequency transformer to provide any electrical isolation between source and load [1].

It consists of six converter topologies :

- Bidirectional Buck-Boost converter
- Cascaded Bidirectional Buck-Boost converter
- Bidirectional CUK converter
- Bidirectional SEPIC-ZETA converter
- Switched Capacitor Bidirectional converter
- Interleaved Non-Interleaved Bidirectional converter

1.4.4.2 IBDC

In IBDC, high frequency transformers are used to provide galvanic isolation. Galvanic isolation is necessary in many applications for safety of source in overload condition, for noise reduction, for voltage matching between conditions .

IBDC are further classified into two topologies .

- Dual Half Bridge (DHB)-Isolated BidirectionalConverter .
- Dual Active Full Bridge (DAFB) Isolated Bidirectional Converter .

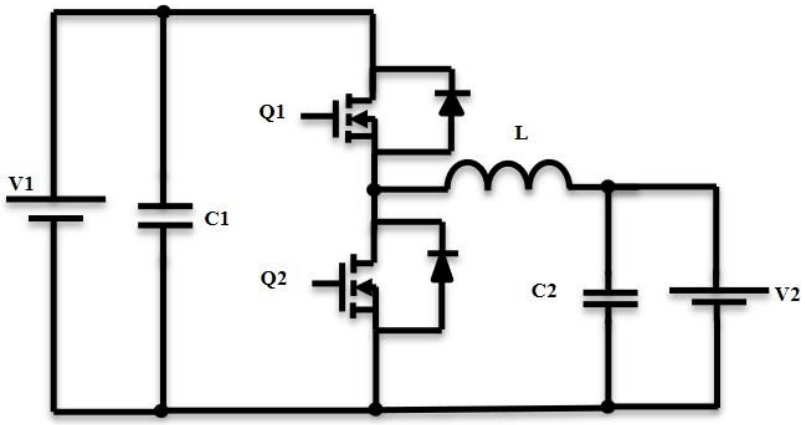

Fig. 1.4 Bidirectional Buck-Boost Converter

In our proposed work a **synchronous bidirectional half-bridge buck-boost converter** is employed. This converter facilitates a constant DC supply of 400 V to the motor. The switching action of Q1 and Q2 in the circuit produce the duty cycle required to increase or decrease the output voltage. The design and operation of this model is discussed in the subsequent chapters .

1.5 CONTROLLERS

It is responsible for the performance of the control system. It is a device or an algorithm that works to maintain the value of the controlled variable at a set point. A control system can control its output(s) to a particular value or perform a sequence of events or perform an event if the specified conditions are satisfied based on the input(s) given. The controller receives the difference between the reference set point and the measured output (known as error) and generates a control action to make the error zero . The generated control action manipulates the process variable closer to the setpoint .

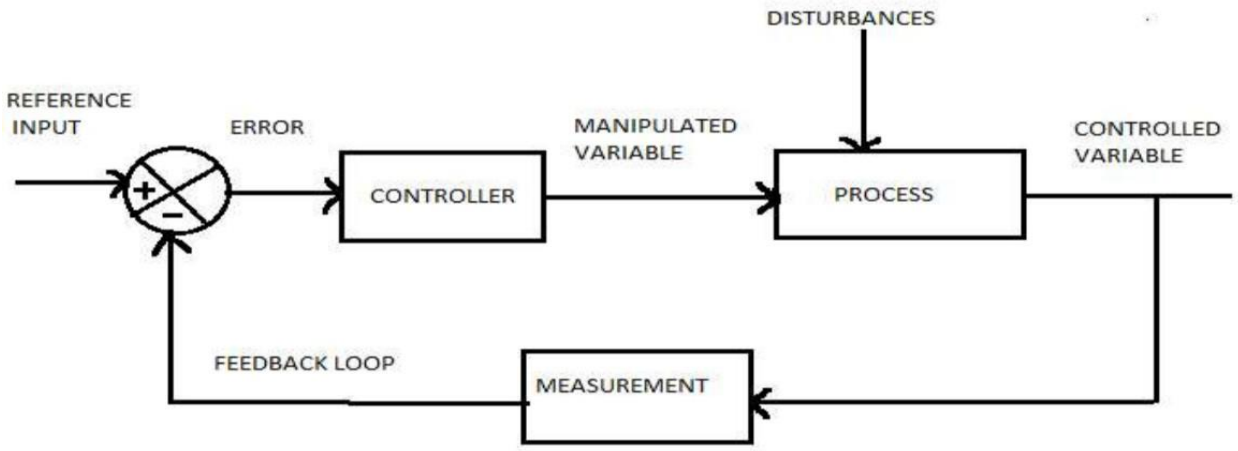

Fig. 1.5 Structure of a Closed-Loop Controller

The various types of controllers are :

- Proportional Controllers
- Integral Controllers
- Differential Controllers
- Fuzzy Logic Controller

1.5.1 PROPORTIONAL CONTROLLERS

Proportional controllers give an output to the actuator which is a multiple of (proportional to) the error . Their response is based on the size of the error. The multiplying factor is the gain which is the change in the output to the change in input. All proportional control systems usually have a steady-state error. The proportional mode of control is generally used in processes where the gain K_p can be made large enough to reduce the steady-state error to an acceptable level.

1.5.2 INTEGRAL CONTROLLERS

The integral term helps to reduce the oscillations and steady-state error. Thus using an integral term along with a proportional controller will result in a better response. As the K_i value increases better is the response.

1.5.3 DERIVATIVE CONTROLLERS

The derivative is concerned with the rate-of-change of the error with time . If the measured variable approaches the setpoint rapidly using K_d, then the actuator is backed off early to allow it to coast to the required level; conversely. if the measured value begins to move rapidly away from the setpoint, extra effort is applied - in proportion to that rapidity to help move it back.

1.5.4 FUZZY LOGIC CONTROLLERS

Fuzzy logic utilizes fuzzy sets to control a particular system. A membership function consists of the error signals that act as the controlling parameters in a system. Using Boolean functions, the certain rules are formulated by evaluating the operating conditions and desired output. The main advantage that oscillations induced by P, PI and PID controllers can be minimized and the steady state can be reached at a much faster rate .

1.6 BLOCK DIAGRAM

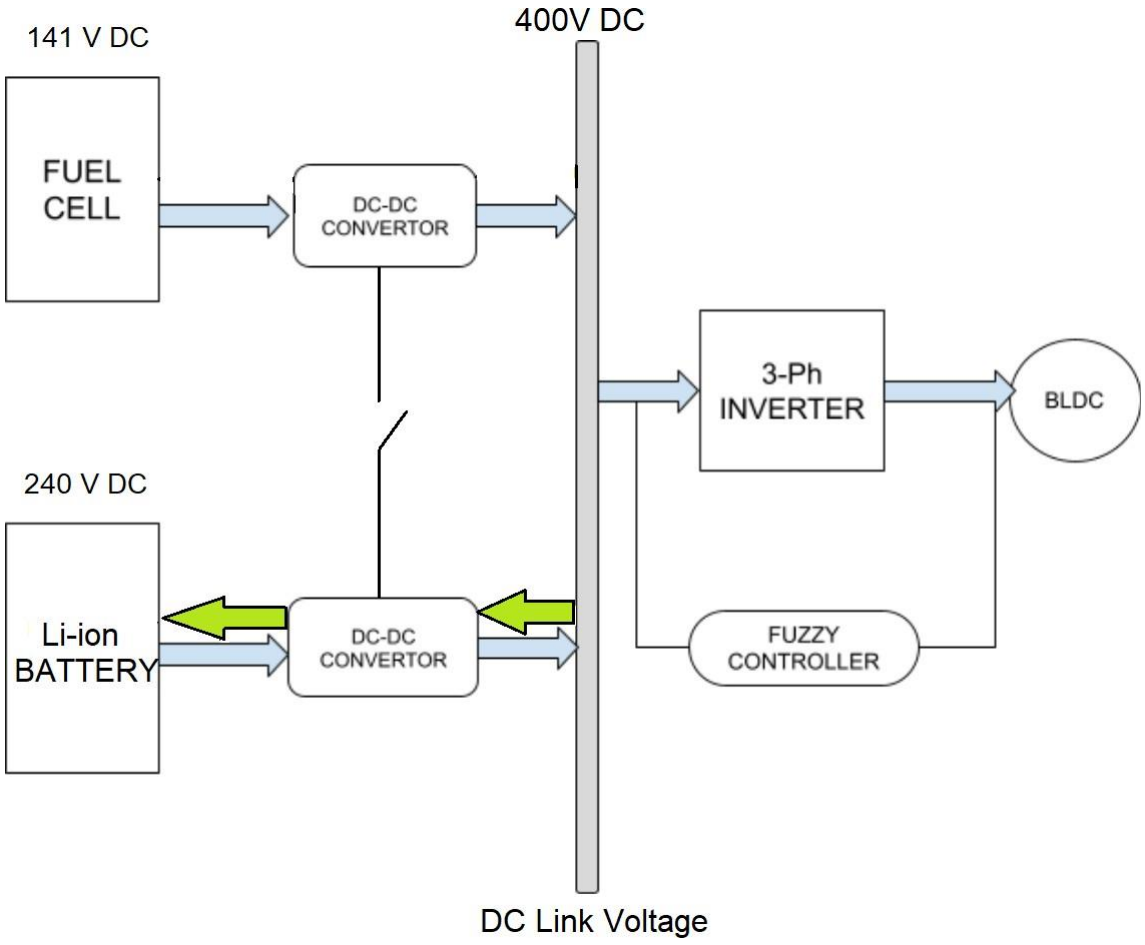

Fig. 1.6 Block Diagram of Proposed Control System

The blue arrows indicate the flow of power from source to load whereas the green arrows indicate the flow of power from load to source . The flow of power to the load is altered through cycles of charging and discharging of the fuel cell and battery respectively. This operation is facilitated by the DC-DC converter . The Fuzzy controller brings out the speed control in the BLDC motor .

1.7 OBJECTIVE

- To design an converter to produce constant voltage using fuel cell as a varying source
- To design a controller to obtain reduced ripples in voltage and current waveform and to maintain a constant DC link voltage for the BLDC motor drive system
- To obtain smooth speed control even at dynamic load conditions using Fuzzy logic controller .

CHAPTER 2

LITERATURE SURVEY

Xuesong Zhou (2016), discusses the studies on the government policies, charging methods, key techniques, impacts of charging, and solutions to the related issues . Based on the current development status and problems, discussing the trend of EV. He introduces briefly some aspects of EV, including random charging and discharging behaviour which brings new challenges to safe and stable operation of power grids. He concluded that the development of EV charging technology has brought a certain opportunity to the safe operation of the network, and how to control the charging and discharging behavior of a large number of EV, which makes the power grid safe and economic operation, it also an important issue [11].

Peter Treffinger(2006), points out that the key issues are cost reduction; higher power density of the primary energy converter, the fuel cell; wider operation ranges and improvement of operation parameters, e.g. higher operation temperature and starting ability in freezing conditions. He provides a short introduction to the technology of fuel cell vehicles and the most prominent fuel cell type for traction applications, the polymer-electrolyte-membrane fuel cell (PEFC). Progress in material development of a core component of the PEFC, the bipolar plate is described. He discusses suitable on-board storages for hydrogen like compressed gas storages and new developments in materials for solid state hydrogen storage are brought to attention. He concluded that DLR concept for compressed gas storage could help to solve the cost and capacity issue together. However, it will be first

applied to compressed natural gas vessels. Further extension of the concept to hydrogen vessels will be an extreme challenge [18] .

Mustafa A. Mhawesh (2006), proposed a detailed study for the response of angular position of the rotor of a DC motor. Modification PID controllers were proposed in this paper. The modification PID controllers are PI-D controller and I-PD controller. Mathematical calculations were done to get the transfer functions for the DC motor and the controllers. This paper determined which the controller is the best one depending on the obtained figures and the time domain specifications. He concluded with four cases of step response angular position of the rotor of the DC motor. The cases are step response with unity feedback control system, step response with conventional PID controller, step response with PI-D controller, and step response with I-PD controller. The time domain specifications for each case was acquired. The best controller was determined depending on the comparison [17].

Faddel, Samy& Mohamed, Ahmed & Mohammed, Osama. (2017), discusses Integrating a fleet of electric vehicles (EVs) in the distribution system without a communication infrastructure exhibits several issues that need to be handled by electric utilities. Robust autonomous controllers are crucial in this case to manage the charging operation without violating the grid standard limits. This paper proposes a communication-free autonomous charging controller for EVs in distribution systems. The controller is based on fuzzy logic considering both the system voltage profile and the EV's battery state of charge (SoC). The fuzzy inference system is designed to avoid under voltage issues in the grid, flatten the system loading profile and accomplish fair charging among different EVs

connected to the system. An 18-bus distribution system driven by the proposed controller was implemented in a simulation environment. The proposed controller performance was investigated under different distribution system operating conditions such as different loading, different levels of EV penetration, system reconfiguration as well as with distributed generation. In all cases, the controller demonstrated faster and better charging performance without violating the standard voltage limits compared to other research reported in the literature [7].

M. Amirabadi and S. Farhangi, Fuel Cell Electric Vehicles (FCEV) have higher efficiency and lower emissions compared with the internal combustion engine vehicles. But, the fuel cell has a slow dynamic response; therefore, an auxiliary power source is needed during start up and transient conditions. Batteries and ultracapacitors can be used as auxiliary power sources. Batteries have high energy density and ultracapacitors have high power density. By using both the battery and ultracapacitors as the auxiliary power sources of the FCEV, the performance and efficiency of the overall system can be improved. In this system, there is a boost converter, which steps up the fuel cell voltage, and two bi-directional DC-DC converters, that each of them couples the battery and ultracapacitors to the bus. Each bi-directional converter has two modes of operation. During the buck mode the battery / ultracapacitors will charge through the fuel cell or regenerative braking. During the boost mode they will supply the load. These converters should be properly controlled. Besides, a control strategy is needed to select the most suitable power source for supplying the load at each operating point, due to the efficiency of the system and demanding power. In this paper the fuzzy control method has been employed for controlling the whole system. Three kinds of fuzzy controllers are needed for this system. One of them is the main controller,

which selects the switches that should be activated at each moment. The second one is the boost controller, which has three inputs and is needed for three switches [15].

Kim, Taehyung & Yang, Jingan. (2009), studies the control of a brushless DC motor/generator in a light motorcycle powered by fuel cell energy for mass production. The zero emission vehicle development will improve air quality and protect the environment. The control strategies for motoring and regenerative braking operations of a brushless DC motor are explained in detail based on a system hybrid control of a fuel cell hybrid vehicle. A prototype experimental test-bed is built for experimental verifications and results are discussed [22].

Uddin, Kotub&Picarelli, Alessandro &Lyness, Christopher & Taylor, Nigel & Marco, James. (2014)., a novel acausal and reconfigurable battery pack model is presented. The model structure adopted for the battery cell is based on an equivalent circuit representation. The circuit elements are modified to take account of both hysteresis and diffusion limitation. The latter is known to be a nonlinear function of large operating currents or long operating times. It is shown that the integration of a current dependent time constant within the cell model better emulates the solid diffusional dynamics of lithium intercalation into the active material under large electrical loads. The advantages of an acausal modelling approach, when scaling-up individual cell models into a complete battery system are also presented. Particular consideration is given to emulating the impact of cell to cell variations on pack performance. Using statistical analysis of battery tests, cell model parameter variations are characterized and quantified. The cell and scaled-up pack model are parameterized for a number of commercially available cell formats, energy capacities and chemistries. The new models are validated using transient,

real-world, electrical data measured from an electric vehicle (EV) operating within an urban environment [13] .

L. Navinkumar Rao and S. Gairola (2016) made a comparative review of bidirectional de-dc converter topologies given by a number of researchers and proposed a basic bidirectional converter operation scheme for interconnection between two battery systems. The study dealt with control and optimal utilization of two battery storage systems by controlling charging and discharging of battery systems. In the system power can flow from one direction to another or vice versa (i.e) it is bidirectional. They'd conducted an experiment with two batteries, one at a higher potential while other at a lower potential than the former one. The Battery A is operated at 48 V and Battery B is operated at 24 V. The bidirectional converter operates in two modes. a) Forward power flow mode and b) Reverse power flow mode. When power flows from 24 V to 48 V batteries, the bidirectional converter works as a boost converter. In that mode, the 24 V battery acted as source and the 48 V battery acted as load. For power flow from 48 V to 24 V systems the bidirectional converter works as a Buck converter. The proposed scheme dynamically controlled the bidirectional converter for different operating load conditions. They carried out simulations using MATLAB software for control and performance evaluation of Bidirectional converters under different operating conditions. The experimental results showed that when power is flowing from battery-B to battery-A, the bidirectional converter works as a boost converter. The voltage across battery-A had been increasing and current found to be negative which meant that battery-A had been charging. At the same time voltage across battery-B had been decreasing and current was positive which meant that battery B was feeding power to battery-A. When the battery voltage decreases the minimum

boundary limit, the transition of bidirectional converter took place and direction of power flow was reversed. They had concluded that in the case of photovoltaic systems, whenever there was a decrease in the output power there would be a transition of bidirectional converter operation and power would be fed by the battery system to load [24].

Iftikhar, Muhammad & Aamir, Muhammad & Waqar, Asad&Naila, & Muslim, Fahad &Alam, Imtiaz. (2018), presents line-interactive transformerless Uninterruptible Power Supply (UPS) with a fuel cell as the prime energy source. The proposed UPS consists of three major parts (i.e., an output inverter, a unidirectional DC–DC converter, and a battery charger/discharger). Non-isolated topologies of both the unidirectional converter and battery charger/discharger ensure transformerless operation of the UPS system. A new topology of high gain converter is employed for boosting the low voltage of the fuel cell to a higher DC link voltage, with minimum semiconductor count, and high efficiency. A high-gain battery charger/discharger realizes the bidirectional operation between the DC link and the battery bank. Besides, it regulates the DC link voltage during the cold start of fuel cells and keeps the battery bank voltage to only 24 V. A new inverter control scheme is introduced that regulates the output voltage and minimizes the total harmonic distortion for non-linear loading conditions. The proposed control scheme integrates proportional-resonant control with slide mode control, which improves the controller's performance in transient conditions. The proposed UPS system is validated by developing a 1-kVA experimental prototype [9].

A. Platon, S. Oprea, A. Florescu and S. G. Rosu, (2018) ,discusses a solution for a digital PI controller implemented in a synchronous Buck converter used in

constant voltage configuration. In such applications, a digital PI controller can replace a traditional PI compensation network made with analog components. This is an approachable solution because Proportional and Integral blocks can be easily defined following a transfer function which can tune the respective coefficients until a stable DC/DC converter is obtained. The PI terms can be digitally implemented using a microcontroller, and then added to the entire system which must provide an adequate response time, maintain system stability and reduce the output voltage steady-state error. A closed loop control system simulation will confirm the above statements. The main advantage of the digital PI control is that no additional analog components are required, resulting in a higher level of integration, also device calibration can be done more smoothly [14] .

CHAPTER 3

SOURCES

3.1 FUEL CELL OPERATION

A proton exchange membrane (PEM) fuel cell consists mainly of two electrodes (cathode and anode) and an electrolyte in between. Oxygen (from cathode side) and Hydrogen (from anode side) are needed for completion of the reaction. The electrodes are usually made flat and the electrolyte is a thin layer to increase the contact area. The structure of the electrode is porous so that both the electrolyte from one side and the gas from the other can penetrate it. This is to give the maximum possible contact between the electrode, the electrolyte and the gas. When an external load is connected to the fuel cell terminals voltage drops take place to express activation, ohmic and concentration losses .

3.2 FUEL CELL - MATHEMATICAL MODEL

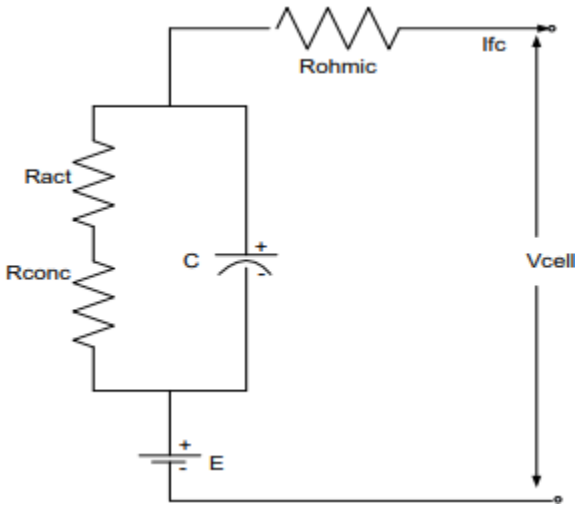

Fig. 3.1 Equivalent Circuit diagram of a Fuel Cell

1) Activation Voltage Drop: Activation voltage drop (ΔV_{act}) is due to the slowness of the reactions taking place in the cell, which can be minimized by maximizing the catalyst contact area for reactions [2]. ΔV_{act} is expressed as

$$\Delta V_{act} = A\ln\left(\frac{i_{fc}+i_n}{i_o}\right) \quad (3.1)$$

Where, A is constant expressed in V .

i_n is the internal current density related to internal current losses expressed in $mAcm^{-2}$ (the importance of the internal current density is much less in case of higher temperature operation with no effect on the fuel cell efficiency). i_{fc} is the output current density given in $mAcm^{-2}$ .i_o is the exchange current density related to activation losses expressed in $mAcm^{-2}$. The activation voltage drop of eqn. (3.1) after removing in is rearranged to

$$\Delta V_{act} = A\ln\left(\frac{i_{fc}}{i_o}\right) = A\ln(i_{fc}) - A\ln(i_o) \quad (3.2)$$

2) Resistive Voltage Drop: Resistive voltage drop (ΔV_{ohm}) is caused by current flow through the resistance of the whole electrical circuit including the membrane and various interconnections, with the biggest contributor being the membrane . Effective water management to keep it hydrated reduces its ohmic loss. ΔV_{ohm} is expressed as :

$$\Delta V_{ohm} = (i_{fc} + i_n)\, r \quad (3.3)$$

Where, r is the area-specific resistance related to resistive losses expressed in Ωcm^2 .

3) Mass Transport or Concentration Voltage Drop: Mass transport or concentration voltage drop (ΔV_{conc}) is caused by gas concentration, which changes at the surface of the electrodes. ΔV_{conc} is expressed as :

$$\Delta V_{conc} = m\exp(n i_{fc}) \quad (3.4)$$

Where, m is constant expressed in V.

n is a constant expressed in cm^2mA^{-1} . ΔV conc can be modelled as a resistance R_{conc} . Equation (3.4) is an empirical one which gives a good fit to fuel cell concentration voltage drop with carefully chosen constants m and n. Then, the fuel cell terminal voltage (V_{cell}) is expressed as :

$$V_{cell} = E - \Delta V_{act} - \Delta V_{ohm} - \Delta V_{conc} \quad (3.5)$$

Where, E is the cell open-circuit voltage at standard pressure and temperature expressed in V.

$$E = -\left(\frac{\Delta h_f}{2F}\right) \quad (3.6)$$

Where, F is Faraday constant, the charge on one mole of electrons, 96,485 Coulombs. Δh_f is the change of enthalpy of formation per mole (= −241.83kj/mol) for water in a steam form and called lower heating value , and Δh_f = −285.84kj/mol for water in a liquid form and called higher heating value. According to the above output voltage equations (3.1-3.4), an equivalent circuit is depicted for the fuel cell, as shown in **Fig. 3.1 .**

In the above circuit, C is the equivalent capacitor due to the double-layer charging effect. The relation between the fuel cell stack voltage and current density is :

$$V_{stack} = N\{E - Aln\left(\frac{i_{fc}+i_n}{i_o}\right) - (\quad i_{fc}+i_n)\, r - mexp(ni_{fc})\} \quad (3.7)$$

Where, N denotes the number of cells in the stack. Because the second half of eqn. (3.2) is a constant, one can deal with this by postulating a real, practical, open circuit voltage E_{oc} that is given by the equation :

$$E_{oc} = E + Aln(i_o) \quad (3.8)$$

Note that E will always be less than E because io , being small, will generate negative logarithms. If we substitute equations (3.2) and (3.8) into eqn. (3.7) and remove in , we obtain .

$$V_{stack} = N\{E_{oc} - Aln(i_{fc}) - (i_{fc})r - mexp(ni_{fc})\} \quad (3.9)$$

Based upon eqn (3.9), a fuel cell model is realized in SIMULINK based on the following parameters. The operating parameters of the fuel cell are given in Table 3.1.

Table 3.1

Operating Parameters of Fuel Cell

Nominal Stack Power	3195 W
Maximal Stack Power	3814 W
Fuel Cell Resistance	2.013Ω
Nernst Voltage of one Cell	1.0562 V
Nominal Hydrogen Utilization	79.54%
Nominal Oxygen Utilization	29.82%
Nominal Fuel Consumption	49.73 slpm
Nominal Air Consumption	59.21 slpm
Exchange Current (i_o)	0.1824 A
Exchange Coefficient (α)	-0.3147
Fuel Composition at signal variation	50%
Oxidant Composition at signal variation	21%
Nominal Hydrogen Fuel rate	148.1 lpm
Maximal Hydrogen Fuel rate	163.9 lpm

Nominal Air Fuel rate	635 lpm
Maximal Air Fuel rate	702.7 lpm
System Temperature	873 K
Fuel Supply Pressure (P_{fuel})	1.35 bar
Air Supply Pressure (P_{air})	1.5 bar

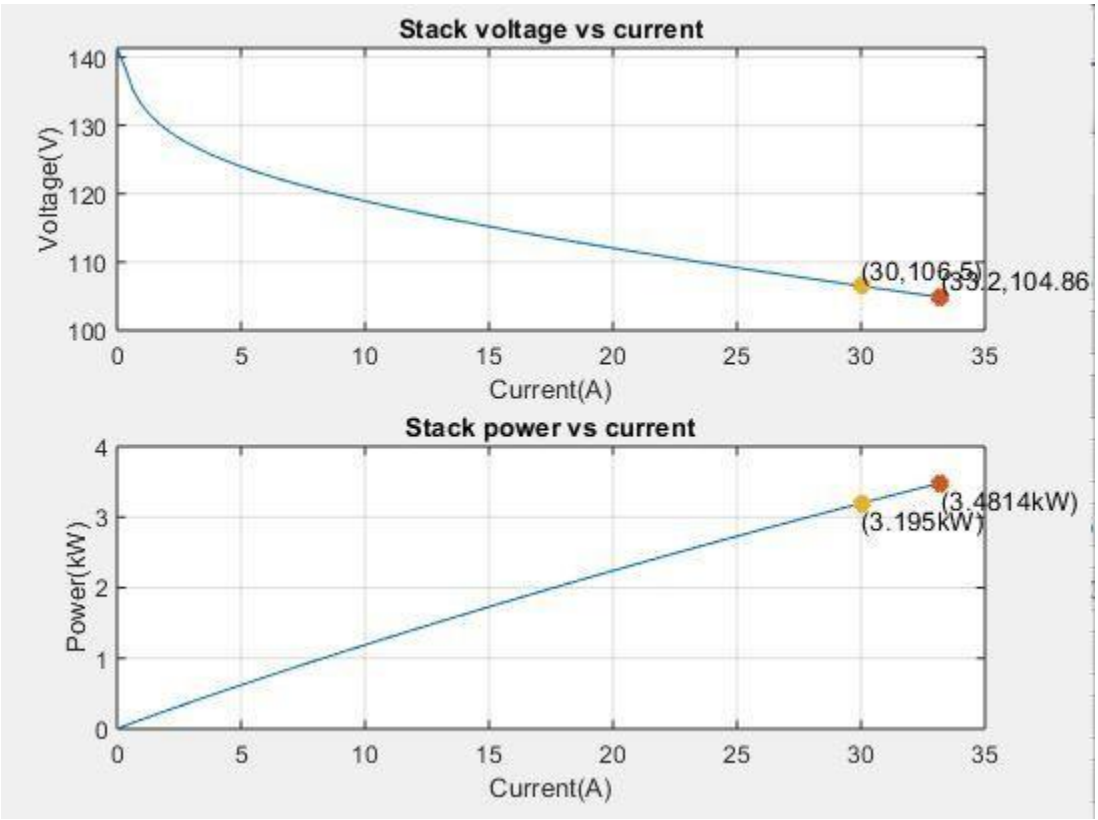

Fig. 3.2(a) V-I characteristics of a Fuel Cell

Fig. 3.2 (b) P-I characteristics of a Fuel Cell

Fig. 3.2(a) shows the V-I characteristics of a Fuel Cell and Fig. 3.2 (b) shows P-I characteristics of a fuel cell based on the operating parameters mentioned in Table 3.1 . This indicates that the fuel cell has a high current density output compared to other DC power sources which is useful in driving dynamic loads (i.e motors) .

3.3 Li-ion BATTERY OPERATION

A battery is made up of several individual cells that are connected to one another. Each cell contains three main parts: a positive electrode (a cathode), a negative electrode (an anode) and a liquid electrolyte. Lithium-ion batteries provide power through the movement of ions. Lithium is extremely reactive in its elemental form that's why lithium-ion batteries don't use elemental lithium. Instead, lithium-ion batteries typically contain a lithium-metal oxide, such as lithium-cobalt oxide ($LiCoO_2$). This supplies the lithium-ions. Lithium-metal oxides are used in the cathode and lithium-carbon compounds are used in the anode and the functional diagram of Li-ion battery is shown if Fig. 3.3

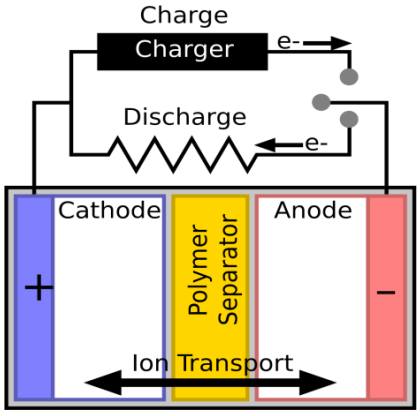

Fig. 3.3 Functional diagram of a Li-ion battery

Inside a lithium-ion battery, oxidation-reduction (Redox) reactions take place. **Reduction** takes place at the cathode. There, cobalt oxide combines with lithium ions to form lithium-cobalt oxide ($LiCoO_2$). The half-reaction is:

$$LiC_6 \rightarrow C_6 + Li^+ + e^- \quad (3.10)$$

Oxidation takes place at the anode. There, the graphite intercalation compound LiC_6 forms graphite (C_6) and lithium ions. The half-reaction is:

$$LiC_6 \rightarrow C_6 + Li^+ + e^- \quad (3.11)$$

Here is the full reaction :

$$LiC_6 + CoO_2 \rightleftarrows C_6 + LiCoO_2 \quad (3.12)$$

When the lithium-ion battery is discharging , positively charged lithium ions (Li^+) move from the negative anode to the positive cathode. They do this by moving through the electrolyte until they reach the positive electrode. There, they are deposited. The electrons, on the other hand, move from the anode to the cathode .The discharging cycle is shown in Fig. 3.4.

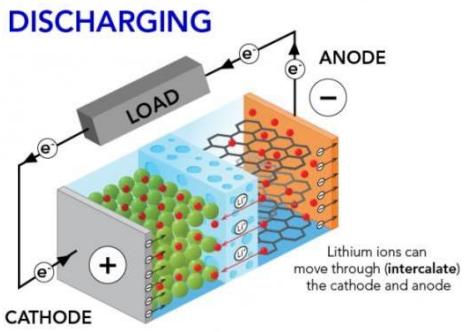

Fig. 3.4 Discharging cycle of a Li-ion battery

When a lithium-ion battery charges, the exact opposite process happens. The lithium ions move back from the cathode to the anode. The electrons move from the anode to the cathode [10] . The charging cycle is shown in Fig. 3.5.

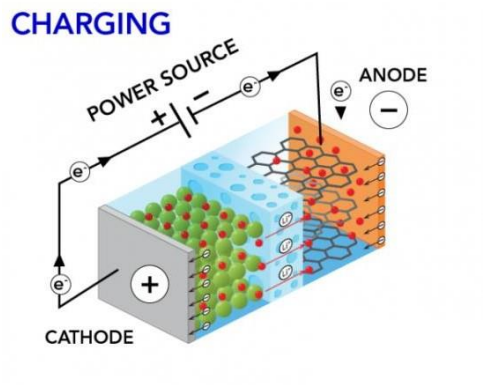

Fig. 3.5 Charging cycle of a Li-ion battery

3.4 Li-ion BATTERY - MATHEMATICAL MODEL

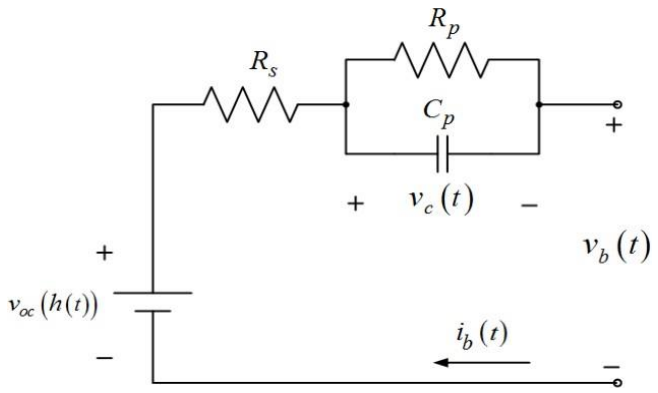

Fig. 3.6 Equivalent Circuit diagram of a Li-ion Battery

In this section, a simple, flexible, and comprehensive semiparametric battery model based on straightforward circuit analysis of the Thevenin equivalent circuit model as shown in Fig. 3.6 . The electrical model is described by an equivalent circuit based on a combination of basic elements, such as voltage sources, resistors, and capacitors, to approximate the electrochemical processes and input-to-output dynamics of the battery [23]. The model consists of

1. The equivalent ohmic internal resistor R_s.
2. The resistor-capacitor (RC) parallel network Cp // Rp (where Rp is the equivalent polarization resistance and Cp is the equivalent polarization capacitance), which is used to simulate transient responses of the battery during charging–discharging transients .
3. The OCV $v_{oc}(h(t))$, which is a nonlinear function of SoC h(t). The equivalent circuit model considers the current as the model control input and the terminal voltage as the measured output.

The equivalent circuit parameters Rs, Rp, and Cp in this model are functions of the temperature and SoC . Using Kirchhoff's law, the dynamics of the circuit can be expressed as follows:

$$v_b(t) = v_{oc}(h(t)) - R_s i_b(t) - v_c(t) \quad (3.13)$$

$$\frac{dv_c(t)}{dt} = -\frac{1}{C_p R_p} v_c(t) + \frac{1}{C_p} i_b(t) \quad (3.14)$$

where $v_b(t)$and $i_b(t)$ are the terminal voltage and current, respectively; and $v_c(t)$is the voltage across the RC network, which cannot be measured directly.

As can be seen from Equations (3.13) and (3.14), the equivalent circuit equations involve the OCV $v_{oc}(t)$ and the polarization voltage,$v_c(t)$ both of which are unknown. However, the unknown term $v_c(t)$ can be removed from these equations based on the following three assumptions :

- The variation in SoC with respect to time is very small because the consumed (or regained) energy is very small compared with the total useful capacity.
- The temperature variation can be ignored for normal operating conditions .
- The usage history of the battery has a long-term effect on battery behaviour, which can be ignored during on-line identification procedure. These assumptions also have been applied in. With the unknown term $v_c(t)$ removed, the dynamics of the battery model can be approximated as follows:

$$\frac{dv_b(t)}{dt} = -\frac{v_b(t)}{C_p R_p} + R_s \frac{di_b(t)}{dt} - \frac{R_s + R_p}{C_p R_p} i_b(t) + \frac{v_{oc}(t)}{C_p R_p} \quad (3.15)$$

The Laplace transformation of (3) can be expressed as follows:

$$V_b(s) = -\left(R_s + \frac{R_p}{1+C_pR_p}\right) I_b(s) + \frac{V_{oc}(s)}{1+C_pR_ps} \tag{3.16}$$

Equation (3.16) is a mathematical model of a continuous system in the s-domain, which can be mapped to its discrete form as follows:

$$v_b(k) = \theta_1 v_b(k-1) + \theta_2 i_b(k) + \theta_3 i_b(k-1) + u(k) \tag{3.17}$$

where $v_b(k)$ and $i_b(k)$ are the samples of $v_b(t)$ and $i_b(t)$, respectively, at time point $t_k = kT_c$ and T_c is the sampling period. θ_1, θ_2, and θ_3 are defined as:

$$\begin{aligned} \theta_1 &= C_pR_p/(C_pR_p + T_c) \\ \theta_2 &= -R_s - R_pT_c/(C_pR_p + T_c) \\ \theta_3 &= C_pR_pR_s/(C_pR_p + T_c) \end{aligned} \tag{3.18}$$

And $u(k)$ is defined as

$$u(k) = (1-\theta_1)v_{oc}(k) \tag{3.19}$$

From (5), the discrete observation equation can be obtained as follows :

$$y(k) = \phi_k^T\theta + u(k) + \varepsilon(k) \tag{3.20}$$

where the superscript T denotes the transpose of a vector or matrix , $\phi_k = [y(k-1), x(k), x(k-1)]^T$ is the measurement vector, is the unknown linear parameter vector, and $\varepsilon(k)$ is assumed to be an additive zero-mean white noise error that contains not only the measurement errors of $v_b(k)$ and $i_b(k)$ but also the interior noise of the battery system.

This way, the dynamics of the OCV of battery using the semiparametric partially linear model .

Based on the above equations, a Li-ion Battery model is realized in SIMULINK based on the following parameters .

3.5 BATTERY PARAMETERS

The Li-ion battery parameters are listed in Table 3.2 .

Table 3.2

Operating Parameters of Li-ion Battery

Nominal voltage (V)	240
Rated capacity (Ah)	5
Initial state-of-charge (%)	80
Battery response time(s)	$1x10^{-4}$
Fully charged voltage (V)	279.3569
Discharge current(A)	2.1739
Capacity(Ah) at nominal voltage	4.5217

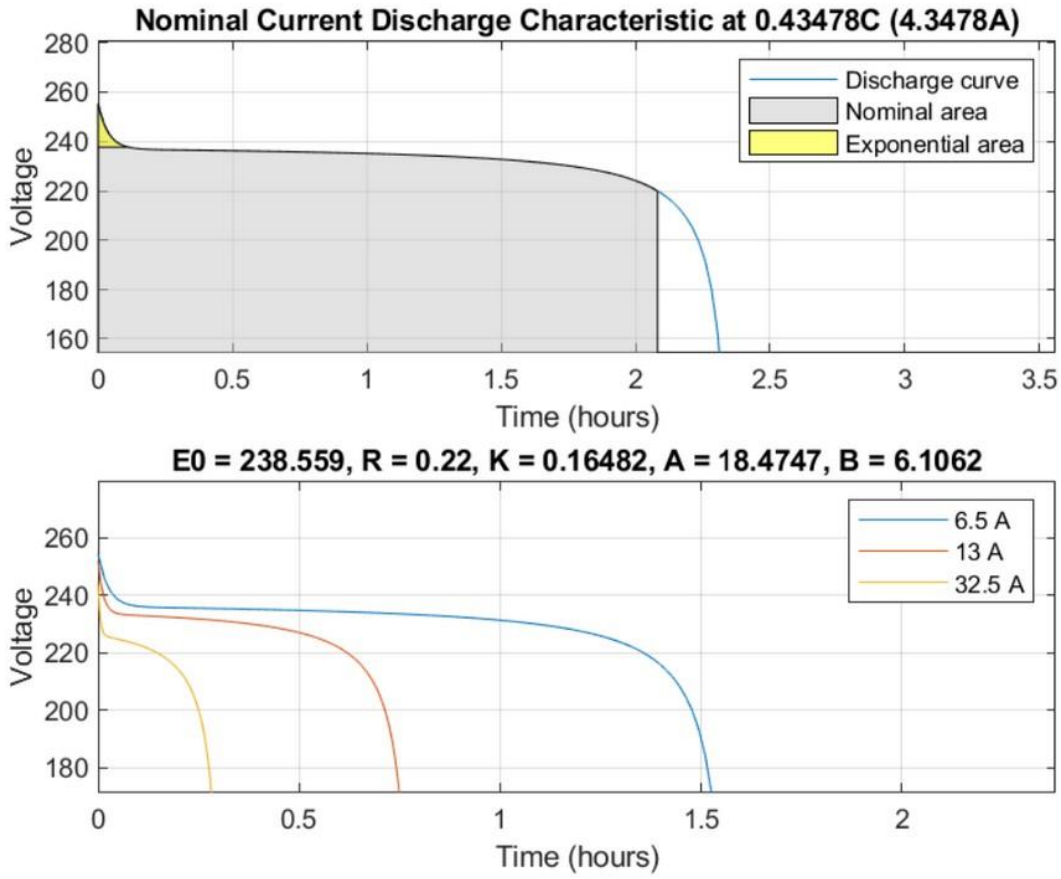

Fig. 3.7(a) Nominal Current Discharge Characteristic of a Li-ion Battery

Fig. 3.7(b) Discharge at Various C-rates of Li-ion Battery

Based upon the values in Table 3.2, Fig. 3.7(a) represents the nominal current discharge characteristic of a Li-ion Battery whereas Fig. 3.7(b) shows the discharge at various C-rates of Li-ion Battery, it can be inferred that the greater the C-rate, the more rapidly the battery discharges .

CHAPTER 4

BIDIRECTIONAL CONVERTER

4.1 INTRODUCTION

A Bidirectional converter is a converter where power can flow in either direction (i.e) power can be supplied to the load from the source or the load (Energy storage loads) can supply power back to the source. As the operating parameters for the fuel cell vary dynamically with respect to the input flow rates of hydrogen (H_2) and air which in turn affect the output voltage on the source side, A bidirectional converter is required to bridge the gap between the load demand and input supply by producing a constant DC link voltage. A similar converter is shown below [21].

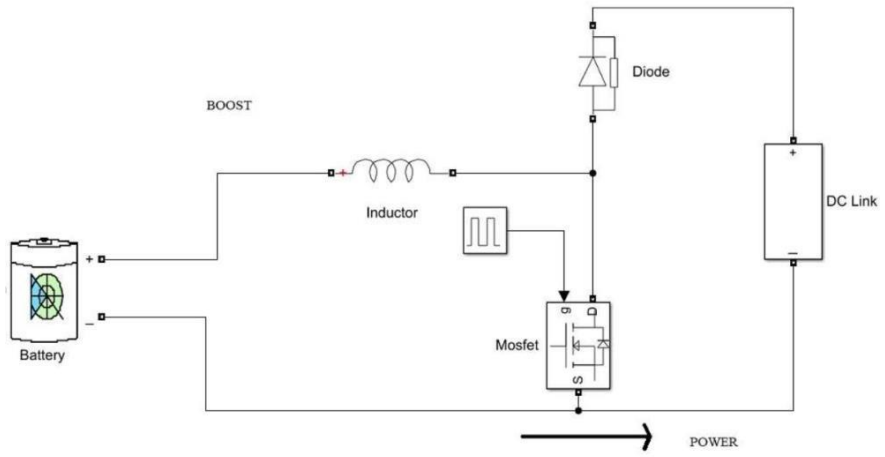

Fig. 4.1 Boost converter SIMULINK model

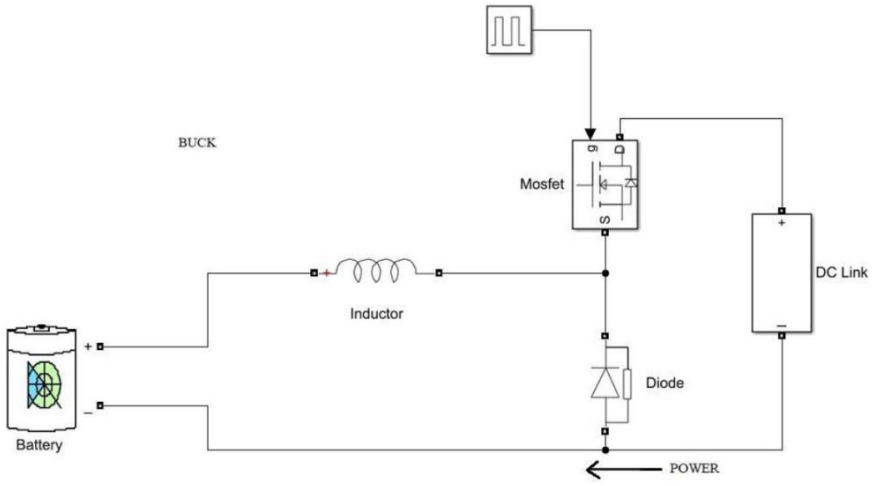

Fig. 4.2 Buck converter SIMULINK model

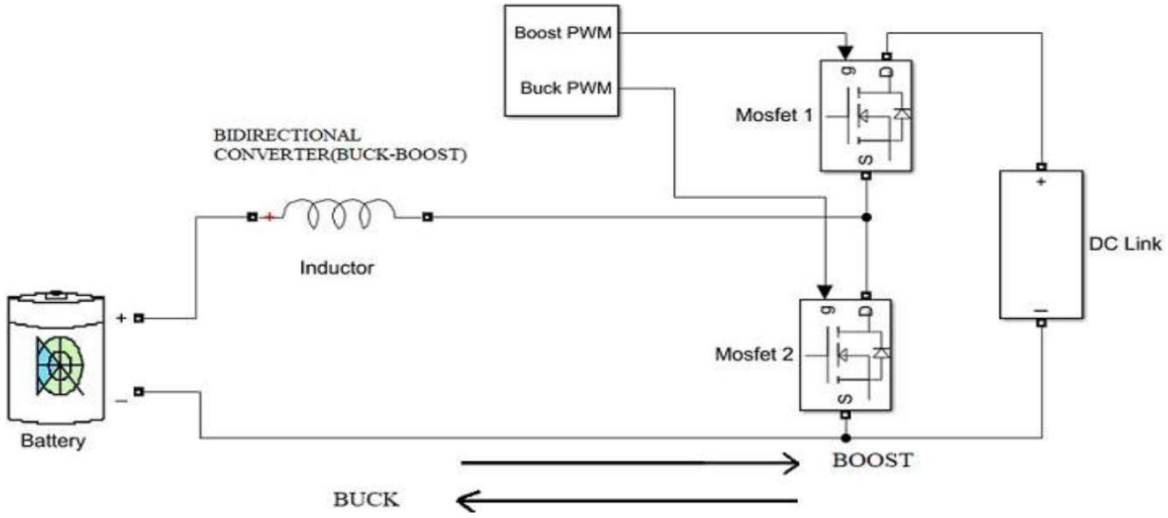

Fig. 4.3 Bidirectional Buck-Boost Converter SIMULINK model

A combination of power electronic switches, inductors and diodes results in a DC-DC converter as shown in Fig. 4.1 and Fig. 4.2. Generation of varying PWM signals to two different MOSFET switches yields a Bidirectional Converter as shown in Fig. 4.3

.

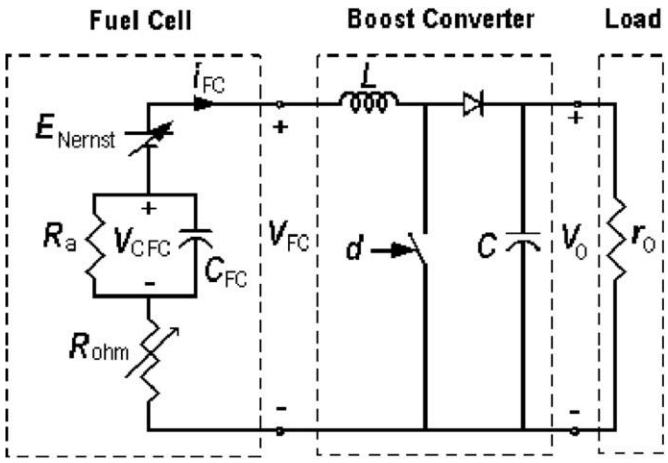

Fig. 4.4 Interfacing Fuel Cell with Boost Converter

The boost converter regulates the fuel cell output voltage to maintain a constant DC link voltage. Fig. 4.4 shows the Interface of the fuel cell with Boost converter.

4.2 WORKING OF BIDIRECTIONAL CONVERTER

The synchronous bidirectional half-bridge buck-boost converter differs from the generic buck-boost convertor in that the output is not inverted and allows power to flow in both directions . Being synchronous means that the duty cycle for both the switches is complimentary, once one switch is conducting the other is blocking and vice-versa [24]. It is composed of two transistors with anti-parallel diodes, an inductor and can have filtering capacitors at each end, which can be seen in Fig. 4.5.

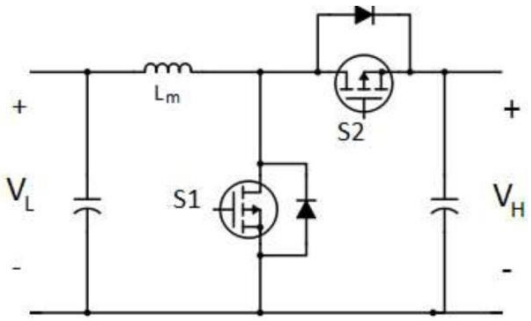

Fig. 4.5 Bidirectional Buck-Boost converter

To get a fundamental understanding of how this topology works a switching analysis of a steady state will be made which describes how the buck and boost mode work. Some simplifications need to be made when explaining DC steady state of the converter such as assuming ideal components, pure DC voltage in V_{in} and voltage V_{out} and operation in continuous conduction mode (CCM) where the inductor current I_L flows continuously .

Table 4.1

Voltage Level Conversion

Mode	**Input voltage**	**Output voltage**	**State of charge**
Buck	240	210	charging
Boost	240	400	discharging

Table 4.2

Design Parameters of DC-DC converter

Load resistance (Ω)	200
Inductance (H)	$1x10^{-3}$
Capacitance (F)	$1x10^{-6}$
Switching Frequency (khz)	10

4.3 BOOST MODE IN BIDIRECTIONAL CONVERTOR

Boost mode is when a lower input voltage is converted into a higher output voltage , or when current flows from the lower voltage side to the higher voltage side. The switching analysis is done in two phases which describe the electrical characteristics of the circuit during switching. In Fig. 4.6 (a) an equivalent circuit can be seen for the first phase, when the switch S1 is conducting and switch S2 is blocking, during the interval

$$0 < t < DT_S \quad (4.1)$$

where D is the duty cycle and T_s is the switching period .

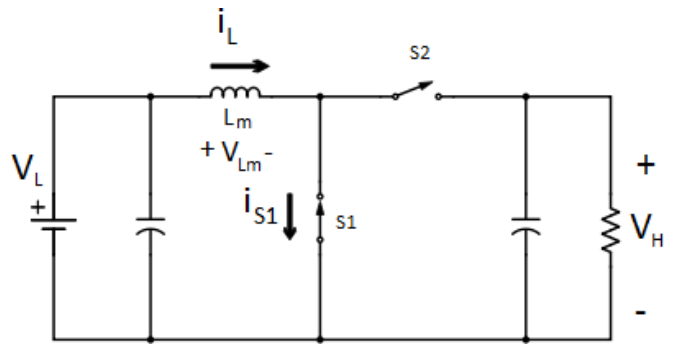

Fig. 4.6(a) First Cycle of Operation in Boost Mode

In this equivalent circuit, the input voltage V_L is applied across the inductor making the input voltage equals the inductor voltage. The constant positive voltage across the inductor makes the inductor current increase linearly, thus increasing the inductor energy. This can be described using the formula

$$v_{L_m} = V_L = L_m \frac{di_{Lm}}{dt} \tag{4.2}$$

Since the inductor current increases linearly, the rate of change of the inductor current during the first phase can be described as

$$\frac{di_{Lm}}{dt} = \frac{\Delta i_{Lm}}{DT} = \frac{V_L}{L_m} \tag{4.3}$$

from which the change of inductor current during the first phase is

$$\Delta i_{Lm1} = \frac{V_L}{L_m} DT. \tag{4.4}$$

By switching S1 and S2 to their blocking and conducting states respectively the second phase is entered. An equivalent circuit for this phase can be seen in Fig. 4.6(b) . This occurs during the interval

$$DT_S < t < T_S$$

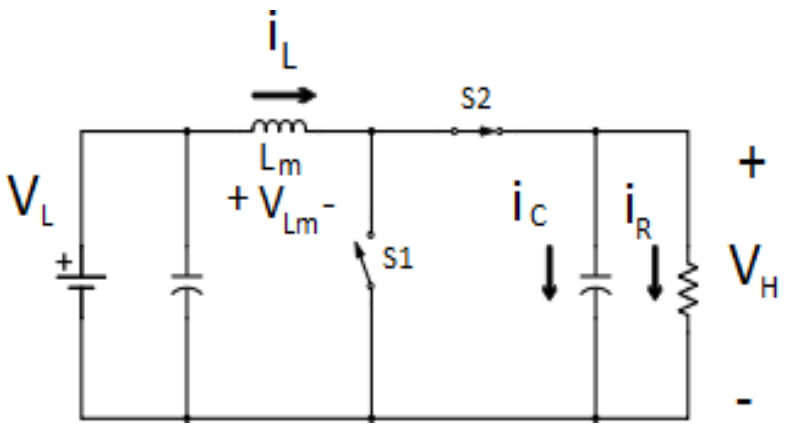

Fig. 4.6(b) Second Cycle of Operation in Boost Mode

During this phase, the input voltage V_L is applied to one side of the inductor, while the output voltage V_H is applied to the other side. This constant negative voltage across means that the inductor voltage will decrease linearly and can be described using the formula

$$v_{L_m} = V_L - V_H = L_m \frac{di_{L_m}}{dt} \tag{4.5}$$

Since the inductor current decreases linearly, the rate of change of the inductor current during the second phase can be described as

$$\frac{di_{L_m}}{dt} = \frac{\Delta i_L}{(1-D)T} = \frac{V_L - V_H}{L_m} \tag{4.6}$$

from which the change of inductor current during the first phase is

$$\Delta i_{L_{m2}} = \frac{(V_L - V_H)}{L_m}(1-D)T \tag{4.7}$$

Since steady-state operation and continuous conduction mode is assumed the total change of current during one switching period equals zero.

$$\Delta i_{L_{m1}} + \Delta i_{L_{m2}} = 0 \tag{4.8}$$

which can be expressed as

$$\frac{V_L}{L_m}.D.T + \frac{(V_L - V_H)}{L_m}.(1-D).T = 0 \quad (4.9)$$

and simplified to

$$V_L.D + (V_L - V_H).(1-D) = 0 \quad (4.10)$$

which can be further simplified to reveal the voltage and duty cycle relation,

$$V_H = \frac{1}{1-D}.V_L \quad (4.11)$$

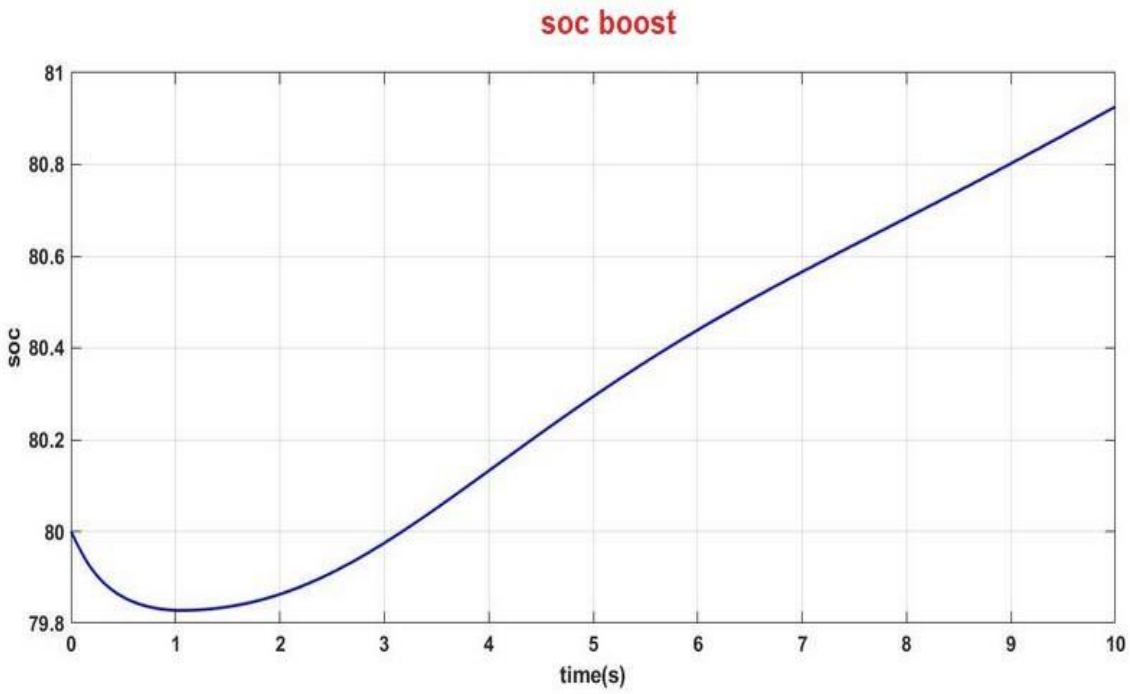

Fig. 4.7(a) Change in SoC of Power Sources during Boost Mode

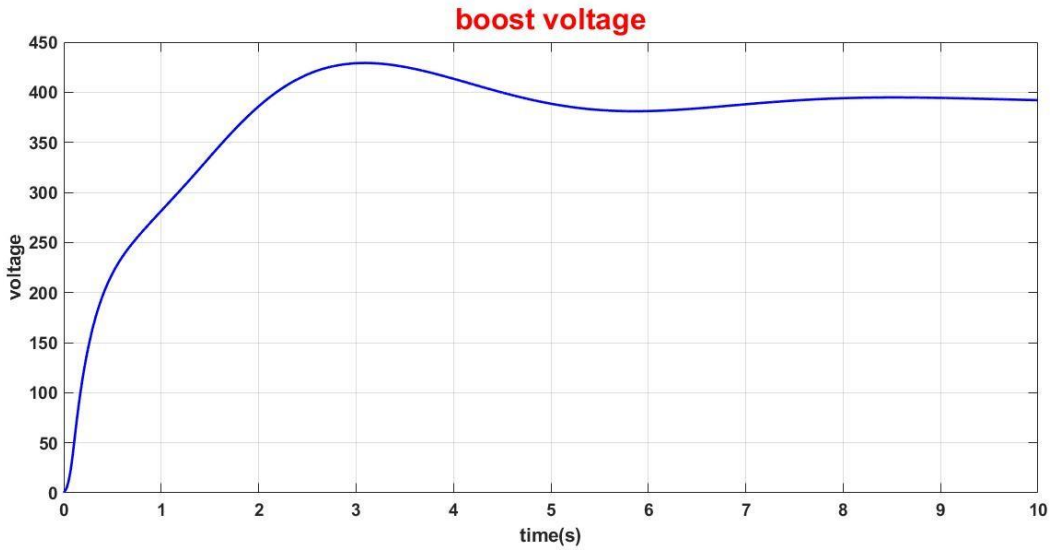

Fig. 4.7(b) Change in Voltage of Power Sources during Boost Mode

Inference : During the Boost operation , the SoC of the power source rises rapidly over a period of 10 s from 80% . Similarly, the voltage rises, peaks over 400 V at t =2.75s and nearly stabilizes at 400 V DC link voltage over a period of 10 s from the fuel cell output .

4.4 BUCK MODE IN BIDIRECTIONAL CONVERTER

The operation of buck mode can be explained in two phases. During the first Phase, as seen in Fig. 4.8(a), the switch S2 is conducting and the switch S1 is off, the current will flow from high voltage V_H to the low voltage V_L through the inductor. The voltage over the inductor will then be

$$V_{Lm} = \frac{dI_L}{dT} L = V_H - V_L \qquad (4.12)$$

where the positive current I_L will lead to a linear increase due to the inductor. The total current change during this period can then be described by

$$\frac{\Delta I_{L(on)}}{\Delta T_1} = \frac{V_H - V_L}{L_m} \qquad (4.13)$$

where the time ΔT1 for the first phase is calculated as the product of the duty cycle D and the time T.

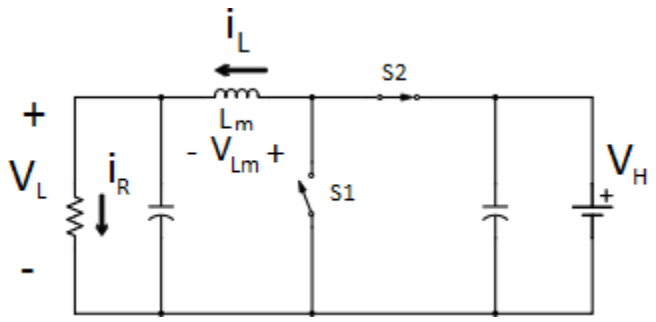

Fig. 4.8(a) First Cycle of Operation in Buck Mode

During the next phase in Fig.4.8(b), the switch S2 is off and S1 is on. This is the same as the inductor is in parallel with V_L but with reversed polarization which means that

$$V_{L_m} = -V_L \tag{4.14}$$

and a negative voltage over the inductor is followed by a negative current derivative. This, in turn, means that the current change during this period can be calculated as

$$\frac{\Delta I_{L(off)}}{\Delta T_2} = \frac{-V_L}{L_m} \tag{4.15}$$

where the time ΔT2 for the second phase will be decided by (1-D)T . By assuming the system to be under steady-state the change of current must be equal to zero during one duty cycle, which means that

$$\Delta I_{L(on)} + \Delta I_{L(off)} = 0 \Rightarrow \frac{V_H - V_L}{L_m} \Delta T_1 + \frac{-V_L}{L_m} \Delta T_2 = 0 \tag{4.16}$$

Since ΔT1 is decided by DT and ΔT2 is decided by (1-D)T the formula concludes in the earlier discussed formula for buck converters being

$$\frac{V_H - V_L}{L_m} DT - \frac{-V_L}{L_m}(1-D)T = 0 \Rightarrow V_L = D.V_H \quad (4.17)$$

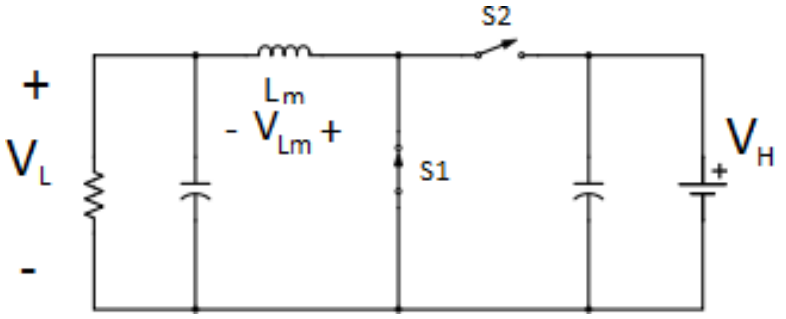

Fig. 4.8(b) Second Cycle of Operation in Buck Mode

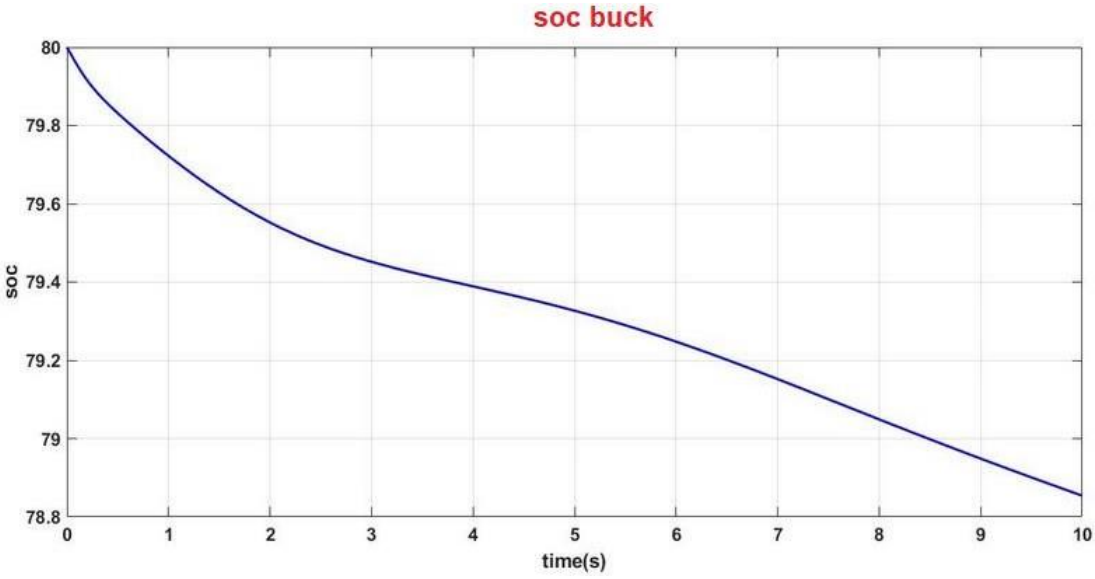

Fig. 4.9(a) Change in SOC of power sources during Buck Mode

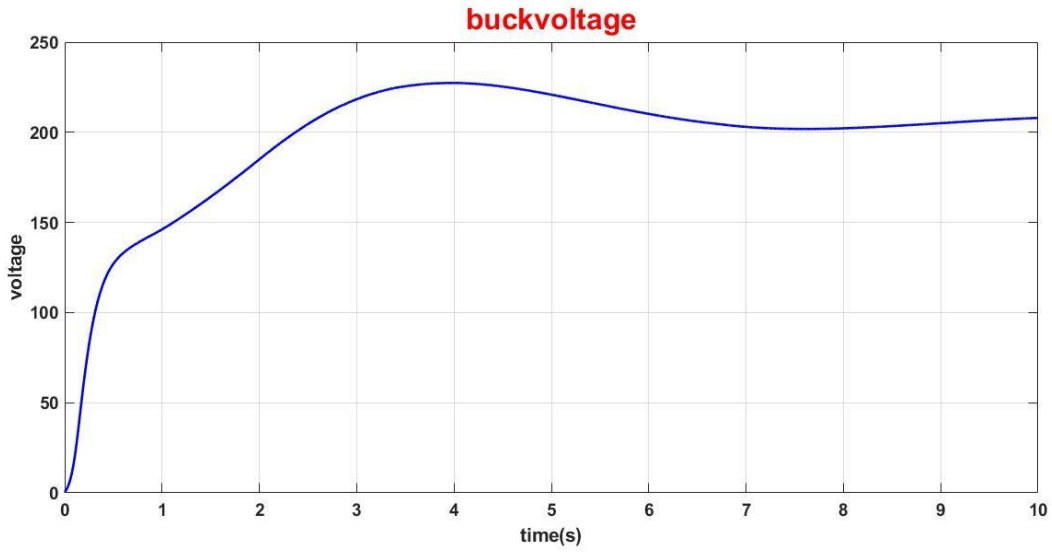

Fig. 4.9(b) Change in Voltage of Power Sources during Buck Mode

Inference : During the Buck operation, the SoC of the power source drops rapidly over a period of 10 s from 80% . Similarly, the voltage will buck from fuel cell input voltage to 210 V at t =2.75s and nearly stabilizes at 210 V DC link voltage over a period of 10 s .

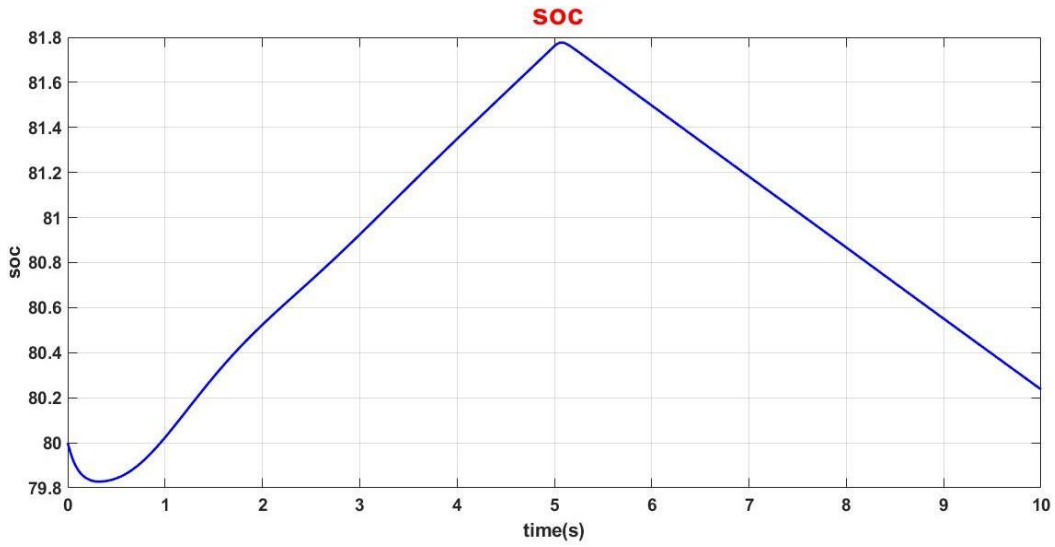

Fig. 4.10(a) Variation in SOC during Buck-Boost operation

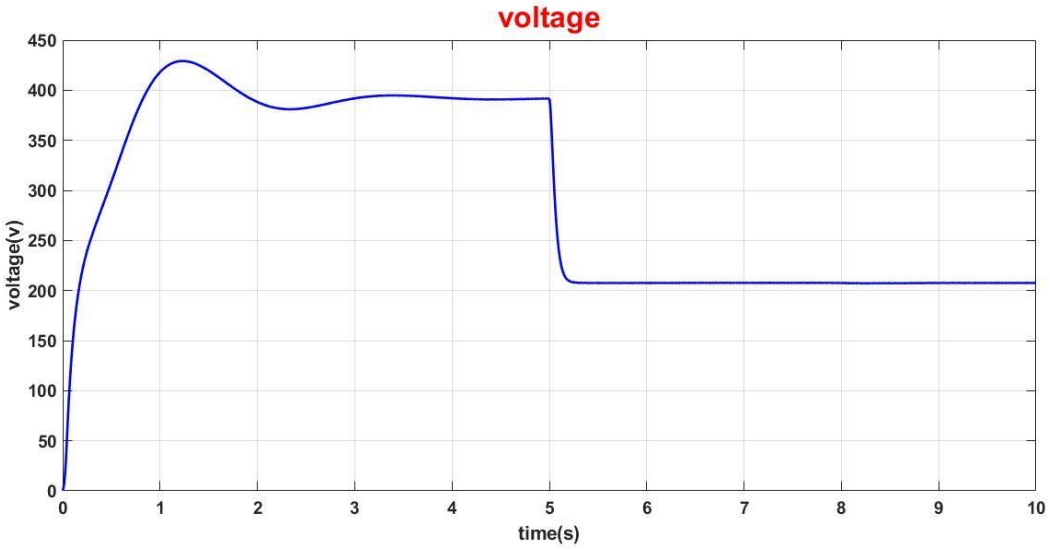

Fig. 4.10(b) Variation in Voltage during Buck-Boost operation

Inference: During the Buck-Boost operation, the SoC of the power source rises rapidly for first 5s from 80% .The SoC of the power source drops rapidly for next 5s from 80% . Similarly, the voltage will rise from fuel cell input voltage to 400 V at t=1s and nearly stabilizes to 400 V DC link over a period of 5s . The voltage drops from 400 V to 210 V at t= 5.2s and nearly stabilizes to 210 V DC link voltage over a period of 10s .

The main goal of the DC-DC converter is to maintain a constant DC link voltage of 400V DC which has been fulfilled to propel our FCEV through traction motors (i.e BLDC motor) discussed in the next chapter .

4.5 SYSTEMATIC POWER FLOW

There are two modes of power flow in the present system .

RED indicates the source is discharging .

GREEN indicates the source is charging .

4.5.1 PRIMARY SOURCE ONLY

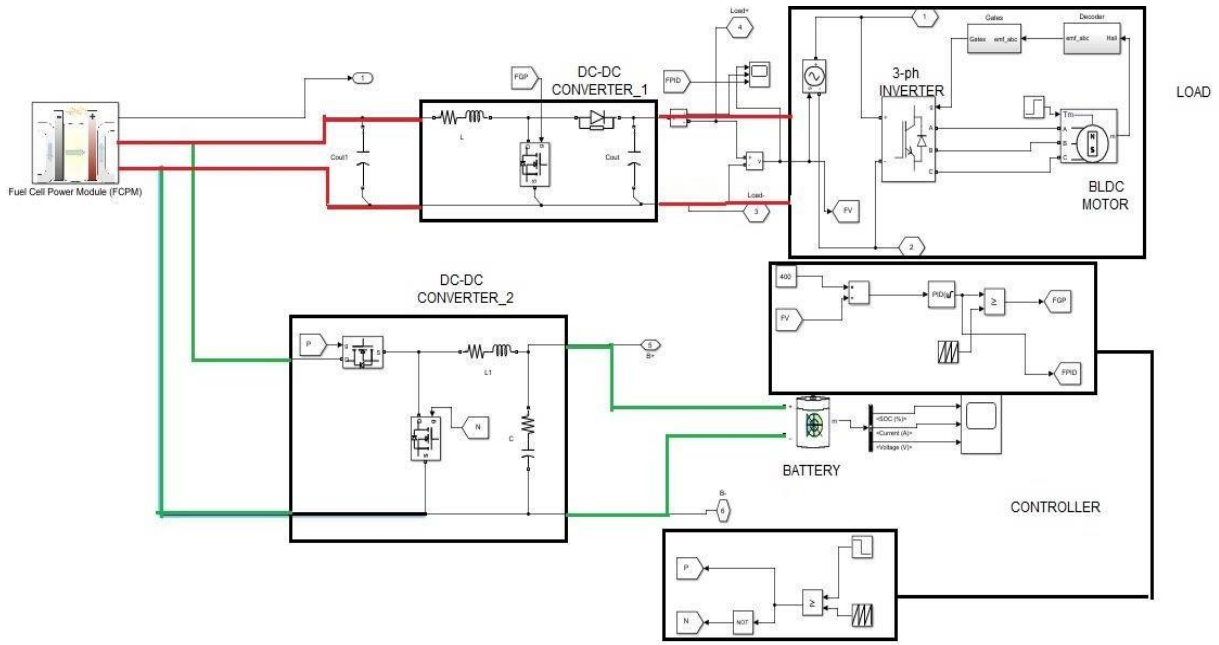

Fig. 4.11 Forward Motoring cum Battery Charging Mode

The Fuel cell helps in propelling the vehicle forward at the same time provides assistance to the auxiliary battery by charging it. In Fig. 4.11 the converter_1 operates in boost mode to maintain a constant DC link voltage to the load block whereas converter_2 operates in the buck mode to charge the battery . Fig. 4.7(a) denotes the rising state of charge in the battery . The controller provides the periodic gate pulses for the smooth operation of the converter .

4.5.2 DUAL POWER MODE

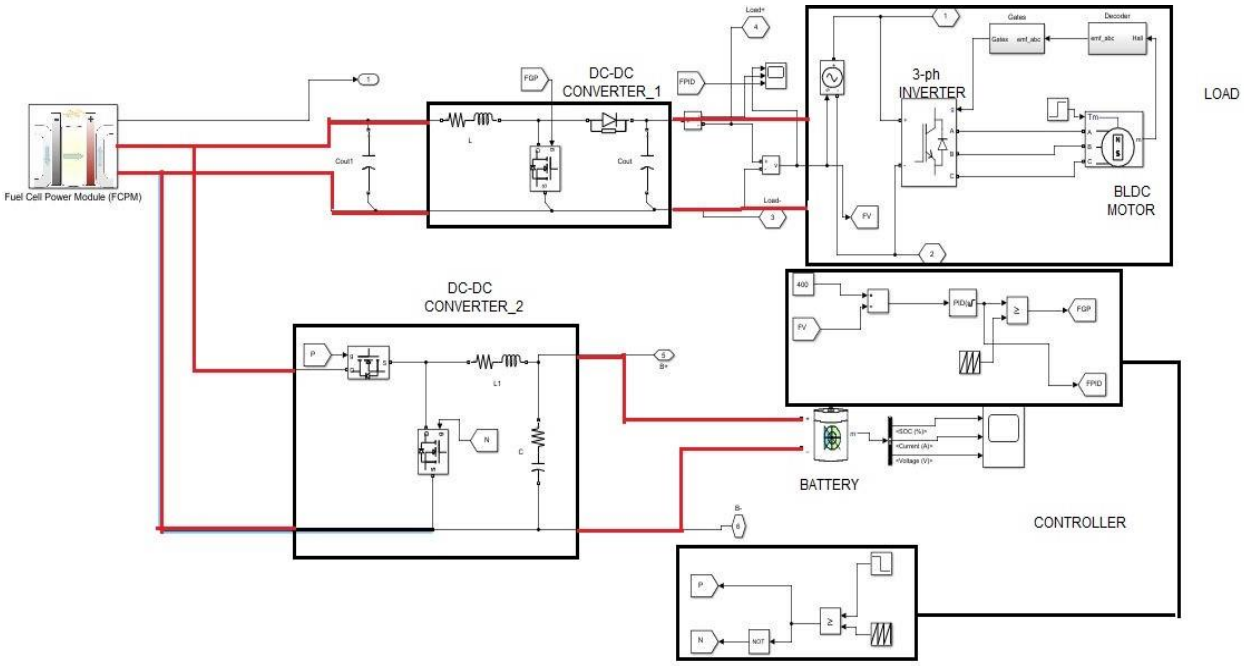

Fig. 4.12 Forward Motoring cum Battery Discharging Mode

The Fuel Cell - Battery combination helps in propelling the vehicle forward simultaneously. In Fig. 4.12, converter_2 operates in the boost mode to discharge the battery . Fig. 4.9(a) denotes the falling state of charge in the battery . During the power cycle shown in Fig. 4.12 the charge accumulated by the battery is harnessed in order to assist the dynamically variable fuel cell to maintain a constant DC link supply of 400 V to the motor. Any operating anomalies are nullified with the aid of the controller .

CHAPTER 5

LOAD

5.1 BLDC MOTOR - MATHEMATICAL MODEL

Modelling of a BLDC motor can be developed in the similar manner as a three-phase synchronous machine. Since its rotor is mounted with a permanent magnet, some dynamic characteristics are different. Flux linkage from the rotor is dependent upon the magnet. Therefore, saturation of magnetic flux linkage is typical for this kind of motor. As any typical three-phase motor, one structure of the BLDC motor is fed by a three phase voltage source. The source is not necessary to be sinusoidal. Square wave or other wave- shape can be applied as long as the peak voltage is not exceeded the maximum voltage limit of the motor. [5] Similarly, the model of the armature winding for the BLDC motor is expressed as shown in Fig. 5.1 .

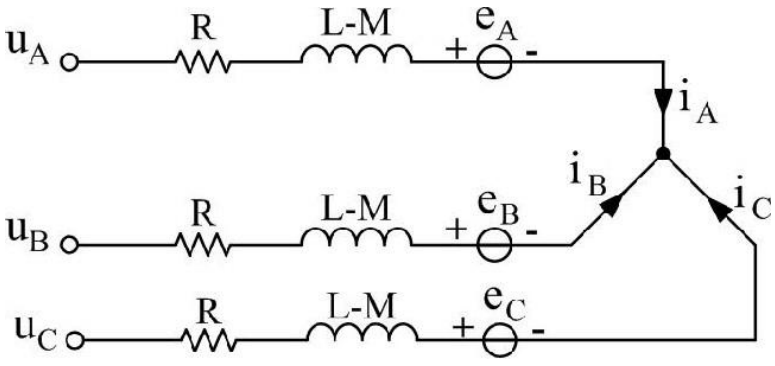

Fig. 5.1 BLDC Motor Equivalent Diagram

$$v_a = R_a + L_a \frac{di_a}{dt} + e_a \quad (5.1)$$

$$v_b = Ri_b + L_b \frac{di_b}{dt} + e_b \quad (5.2)$$

$$v_c = R_c + L_c \frac{di_c}{dt} + e_c \quad (5.3)$$

Where $L_a = L_b = L_c = L = L_s - M$

L_s= armature of self inductance

M =mutual inductance

R_a=R_b=R_c= R = armature resistance in Ω

v_a,v_b,v_c= terminal phase voltage in volts

i_a,i_b, i_c= motor input current in Amps

θ_a, θ_b, θ_c=motor back emf in volts

Due to the permanent magnet mounted on the rotor, its back emf is trapezoidal as shown in Fig. 5.2 . The expression of back emf must be modified as expressed in

$$e_a(t) = K_E \phi(\theta)\, \omega(t) \quad (5.4)$$

$$e_b(t) = K_E \phi\left(\theta - \frac{2\pi}{3}\right) \omega(t) \quad (5.5)$$

$$e_b(t) = K_E \phi\left(\theta + \frac{2\pi}{3}\right) \omega(t) \quad (5.6)$$

Where K_E is the back emf constant and ω is the mechanical speed of the rotor.

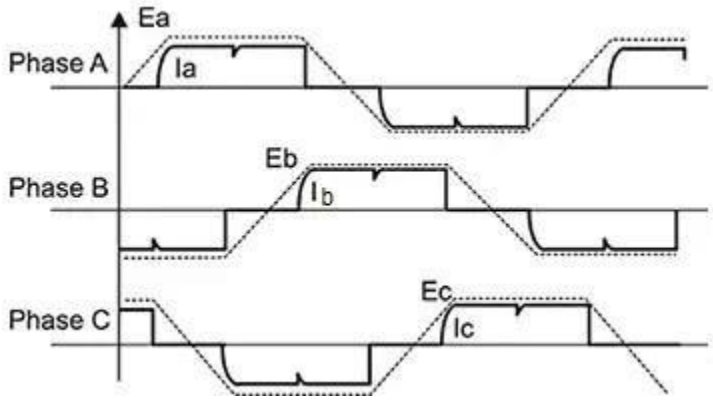

Fig.5.2 BLDC motor per-phase back EMF waveform

$$T_E = (e_a i_a + e_b i_b + e_c i_c) / \omega \quad (5.7)$$

The resultant torque, T_E can be obtained by the following expressions.

$$T_a(t) = K_T \phi(\theta)\, i_a(t) \quad (5.8)$$

$$T_b(t) = K_T \phi(\theta - \frac{2\pi}{3}) i_b(t) \quad (5.9)$$

$$T_c(t) = K_T \phi(\theta + \frac{2\pi}{3}) i_c(t) \quad (5.10)$$

$$T_E(t) = T_a(t) + T_b(t) + T_c(t) \quad (5.11)$$

The permanent magnet also influences produced torques due to the trapezoidal flux linkage. Given that K_T is the torque constant.

With the Newton's second law of motion, the angular motion of the rotor can be written as follows:

$$T_E(t) - T_L(t) = J \frac{d\omega(t)}{dt} + B\omega(t) \quad (5.12)$$

Where,

T_L load torque in N-m

J rotor inertia in kgm

B damping constant

5.1.1 SPEED CONTROL OF BLDC MOTOR

To control the rotor speed in a BLDC based electrical drive. An ideal torque source provides the load. The control subsystem uses a fuzzy-based cascade control structure with an outer speed control loop and an inner dc-link voltage control loop. The dc-link voltage is adjusted through a DC-DC boost converter. The BLDC is fed by a controlled three-phase inverter. The gate signals for the inverter are obtained from hall signals. The simulation uses speed steps.

5.2 AC7-BLDC DRIVE BLOCK

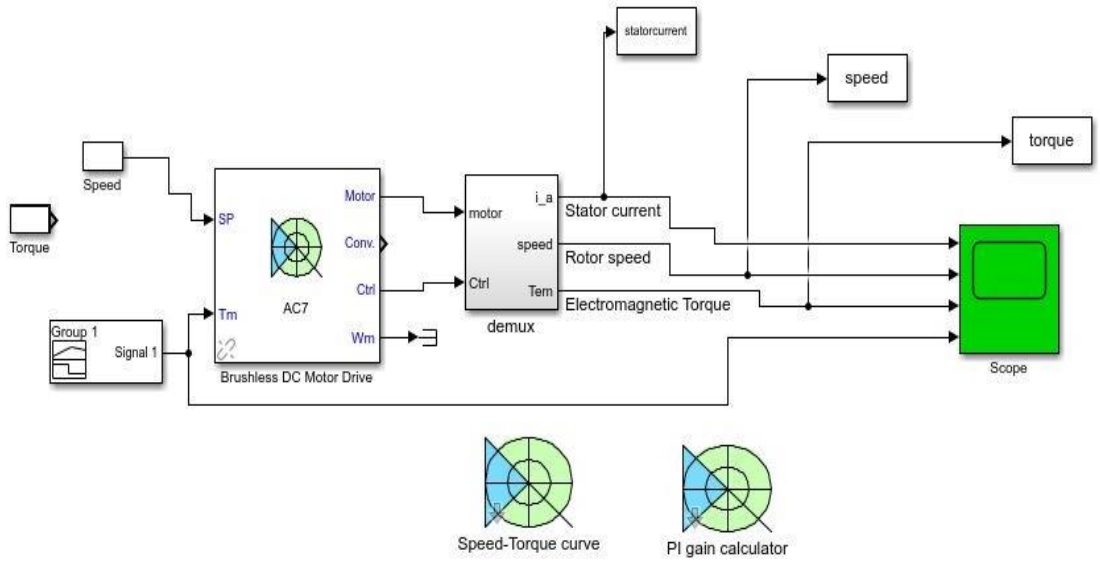

Fig. 5.3 AC7 - BLDC drive block SIMULINK model

5.2.1 LOAD DESCRIPTION

The circuit uses the AC7 block of Specialized Power Systems library. It models a brushless DC motor drive with a braking chopper for a 3HP motor as shown in Fig. 5.3.

The permanent magnet synchronous motor (with trapezoidal back-EMF) is fed by a PWM voltage source inverter, which is built using a Universal Bridge Block [8]. The speed control loop uses a PI regulator as well as a Fuzzy Logic Controller to produce the torque reference for the current control block. The current control block computes the three reference motor line currents, in phase with the back electromotive forces, corresponding to the torque reference and then feeds the motor with these currents using a three-phase current regulator.

Motor current, speed, and torque signals are available at the output of the block. The details of the motor are as compiled in Table 5.1 .

Table 5.1

Operating Parameters of BLDC motor

RATED POWER	3 Hp
RATED VOLTAGE	415 V
RATED CURRENT	4.3 A
RATED SPEED	1500 rpm
RATED TORQUE	3.5 Nm

5.2.2 THREE PHASE INVERTER

An inverter is a type of power electronic device that converts input DC power to output AC power . In general, there are two types of three phase inverters :

- Voltage Source Inverter (VSI)
- Current Source Inverter (CSI)

In the present model, a VSI inverter is implemented and termed as a Universal Bridge in SIMULINK which uses composite switches (IGBT-diode) .

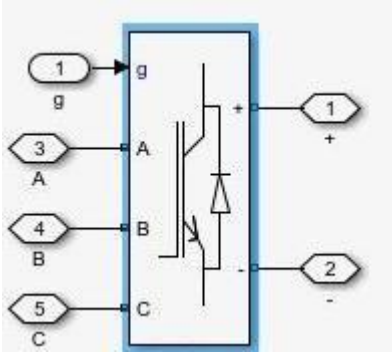

Fig. 5.4 Universal Inverter Bridge (3 arms)

This block implements a bridge of selective power electronic devices as shown in Fig. 5.4. Series RC snubber circuits are connected in parallel with each switch device . The number of bridge arms are 3 with a zero internal inductance value .

The 3-phase output current waveforms from the inverter are shown in the Fig. 5.5.

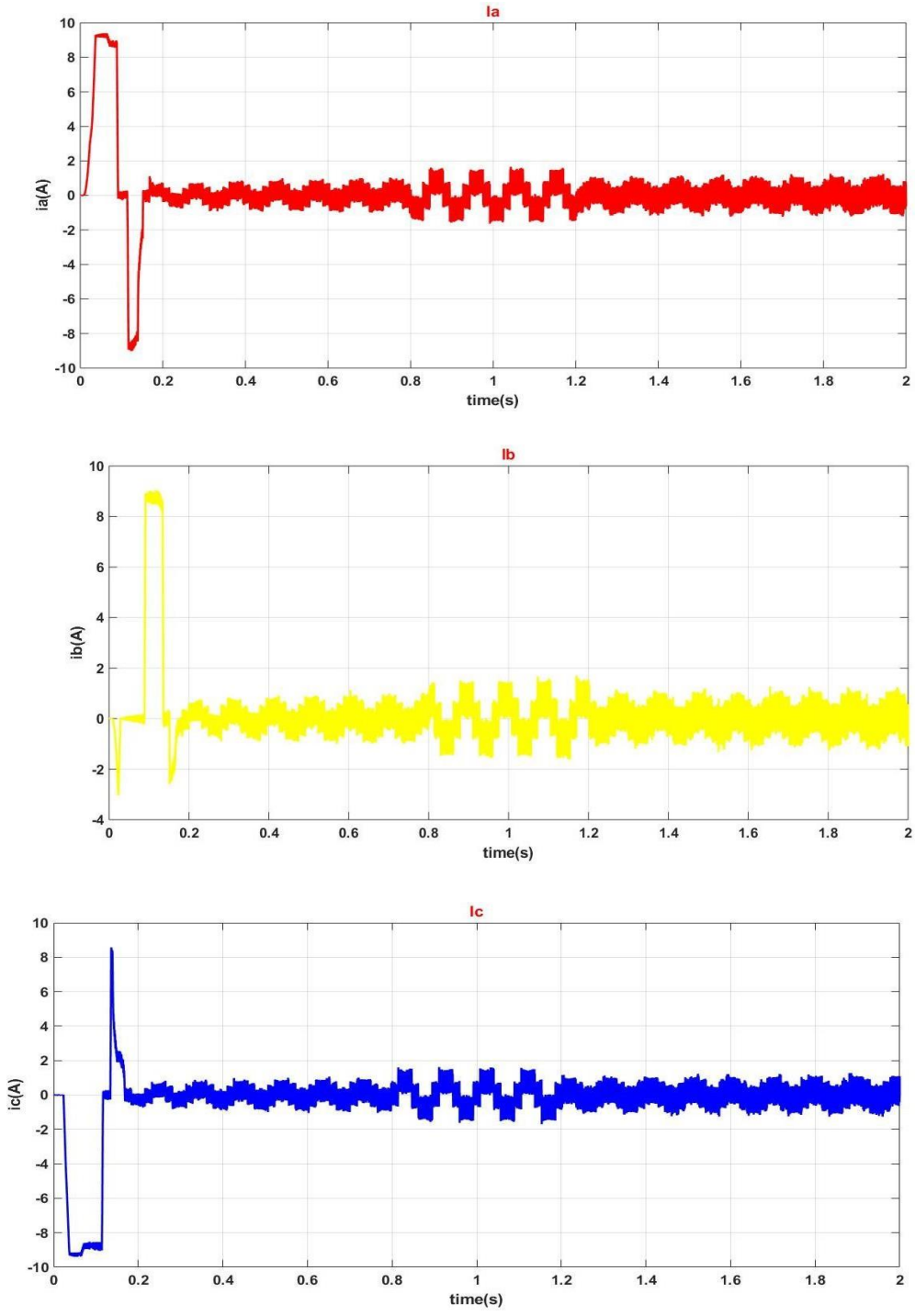

Fig. 5.5 Inverter output waveform (3-phase current)

5.2.3 PMSM

A Permanent Magnet Synchronous Machine (PMSM) implements a three phase machine with the stator winding in a star configuration . The rotor is in a round configuration to facilitate a trapezoidal back emf . The **PMSM** is known for having low torque ripple, superior dynamic performance, high efficiency and high power density. Fig. 5.6 shows a PMSM SIMULINK block .

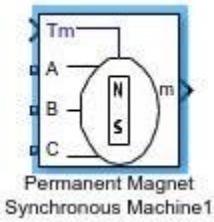

Fig. 5.6 PMSM SIMULINK Block

5.2.4 DEMUX

A demultiplexer performs the reverse operation of a multiplexer. It receives one input and distributes it over several outputs . the demultiplexer takes one single input line and then switches it to any one of a number of individual output lines at a time . A demultiplexer is equivalent to a single pole multi way switch as shown in Fig. 5.7(a). So in order to measure the various speed & torque characteristics of the motor a demultiplexer is implemented based on the input control signal as shown in Fig. 5.7(b).

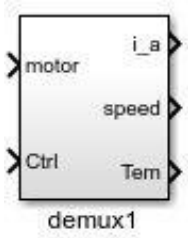

Fig. 5.7(a) Demux SIMULINK block

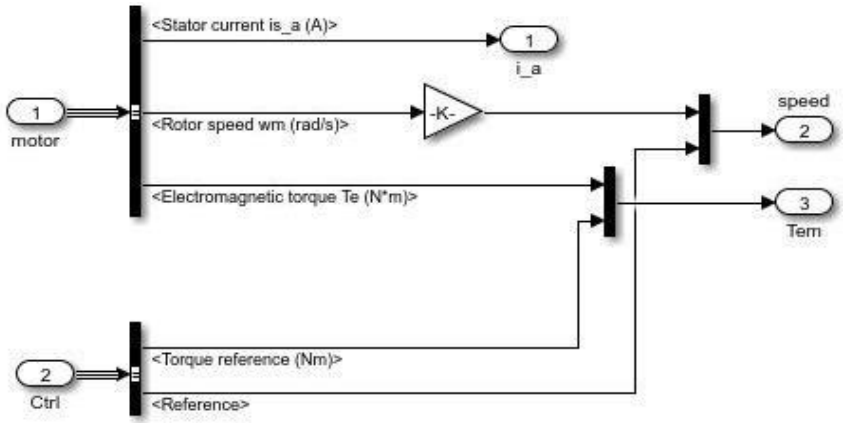

Fig. 5.7(b) Demux control signal and Motor outputs

5.2.5 OUTPUT WAVEFORM

The output waveforms obtained from the BLDC motor as shown in Fig. 5.8.

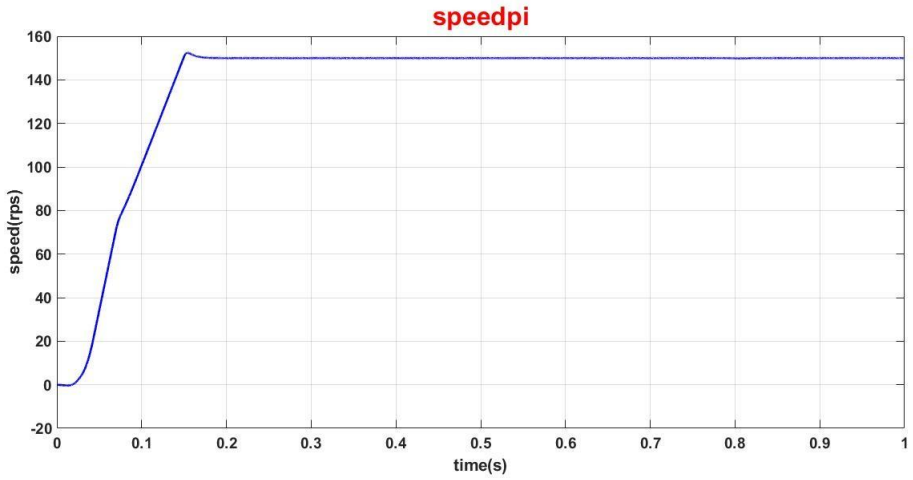

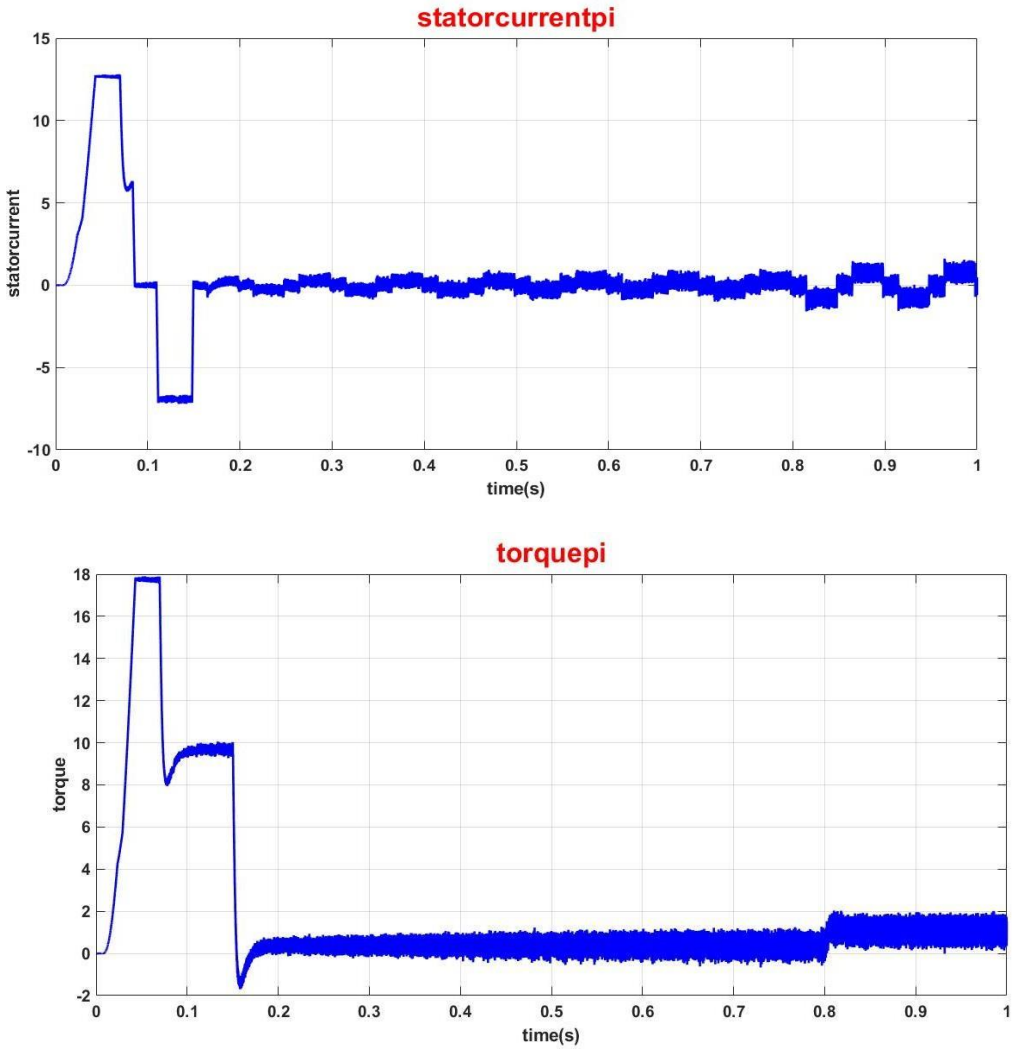

Fig. 5.8 Speed-Stator Current-Torque Characteristics w.r.t Time

Inference : From fig. 5.8 it can be seen that motor characteristics have been simulated . From this, we can observe that initially due to the motor inertia the starting current and starting torque attain a peak value over a transient phase . After this brief period, the motor running characteristics denote that the current and torque values oscillate near zero with some ripples whereas the speed attains a constant value of **155 rad/s** after t=0.17s to t=1s .

CHAPTER 6

CONTROLLERS

6.1 PROPORTIONAL CONTROLLER

Proportional controllers give an output to the actuator which is a multiple of (proportional to) the error. Their response is based on the size of the error. The multiplying factor is the *gain* (= Δ output/Δ input). When the proportional band is too high, a large error value will be required to get the desired output. When the proportional band is too low, a small error will cause a large change in the output that overcompensates; this may send the system oscillating out of control, much like the positive feedback from a public address system. The gain depends on the proportional band expressed as a percentage.

Gain = (100)/ (proportional band in %)

All proportional control systems usually have a steady-state error . Steady state error is nothing but the offset from the setpoint. The proportional mode of control is generally used in processes where the gain K_P can be made large enough to reduce the steady-state error to an acceptable level. However, as the gain increases the tendency of the system to oscillate also increases. The oscillations occur because of time lags in the system, the higher the gain the bigger will be the controlling action for a particular error and so greater is the chance that the system will overshoot the set value and oscillations occur. These are the disadvantages of the P controller.

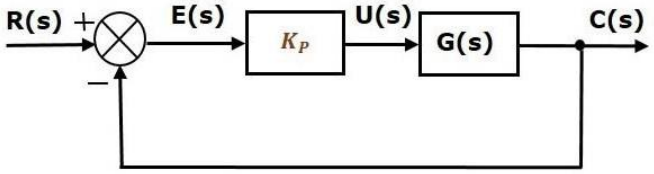

Fig. 6.1 Block diagram of Proportional Controller

$R(s)$ - set point

$C(s)$ - present value

$E(s)$ - error signal

$K_P(s)$ - proportional constant

$U(s)$ - P controller output

$$E(s) = R(s) - C(s) \tag{6.1}$$

$$U(\mathrm{s}) = K_P E(s) \tag{6.2}$$

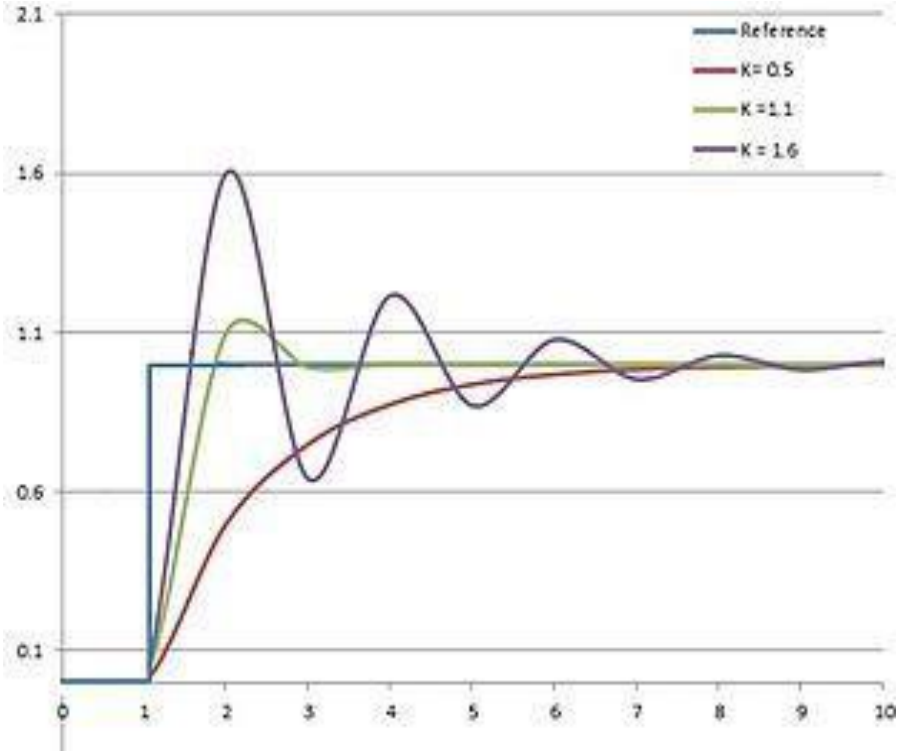

Fig. 6.2 Output Response v Time (Proportional Controller)

The above graph shows the response of the system for different values of K_P . From the above graph it can be seen that higher the value of $K_P$lesser is the steady-state error but we have more oscillations. And in the same way smaller the value of $K_P$larger is the steady-state error but the oscillations are lesser . Thus we go for a PI controller.

6.2 PROPORTIONAL AND INTEGRAL CONTROLLER

The output from the integral controller is a multiple of both the magnitude of the error and the duration of the error . The integral term in the PI controller is the sum of the accumulated error over a period of time and gives the accumulated error which should have been corrected earlier . This accumulated error is then multiplied by the integral constant $K_i$and this is given as the output of the integral controller . Thus the integral controller reduces the steady state error and also reduces the oscillations which occurred while using only the proportional controller.

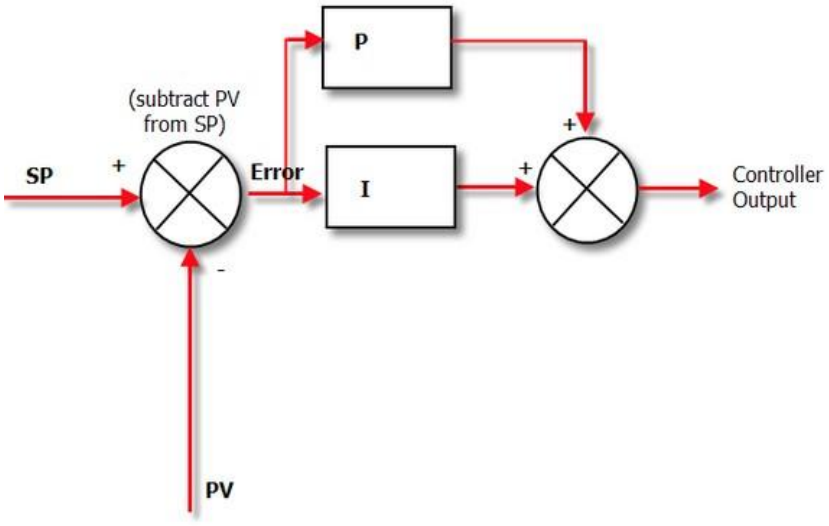

Fig. 6.3 Block diagram of Proportional-Integral Controller

SP - set point

PV - present value

$e(t)$- error

K_P - proportional constant

K_i- integral constant

$U(t)$ - output of the PI controller

$$e(t) = SP - PV \tag{6.3}$$

$$u(t) = u_{bias} + K_c e(t) + \frac{K_c}{\tau_i}\int_0^t e(t)dt \tag{6.4}$$

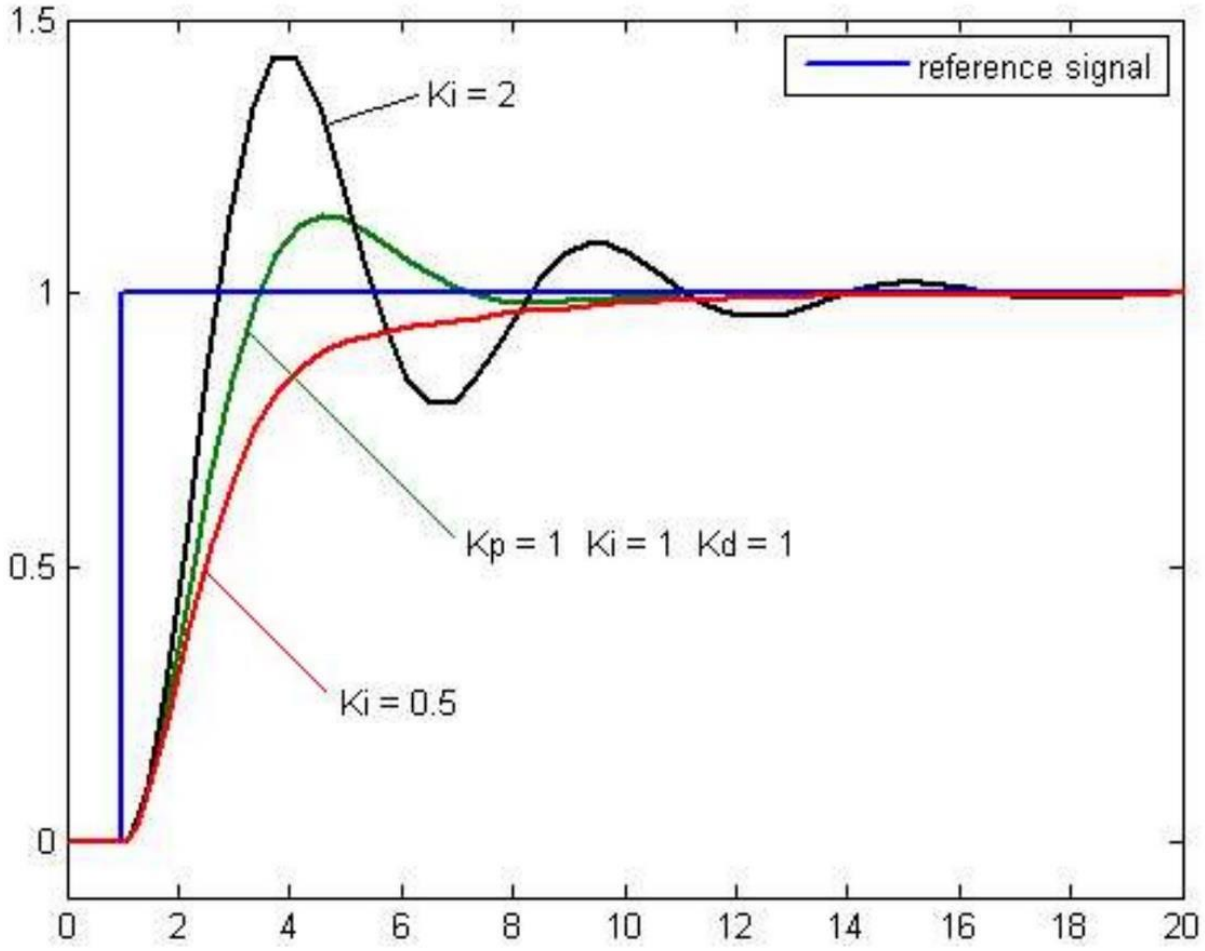

Fig. 6.4 Output Response v Time (Proportional-Integral Controller)

The above graph shows the output response of a system using an integral controller. It can be seen from the graph that when the value of the integral constant (K_i=0.5) is low there is a small steady state error, on the other hand it can be seen that when the when the integral constant is high (K_i= 2) there is an overshoot in the response . But when the integral constant is at an optimum value (K_i= 1) the response doesn't have a steady state error or any oscillations and the response has nearly settled at the point. Similarly, the output response obtained in the real-time simulation of the PI control system follows a similar trend as in Fig. 6.4 where the AC7 BLDC drive block consists of an in-built PI controller .With a desired output speed of 150 rad/s **,**the errors and oscillations encountered are rectified by tuning the controller as shown in Fig. 6.5. In this project we have employed a Fuzzy Logic Controller .

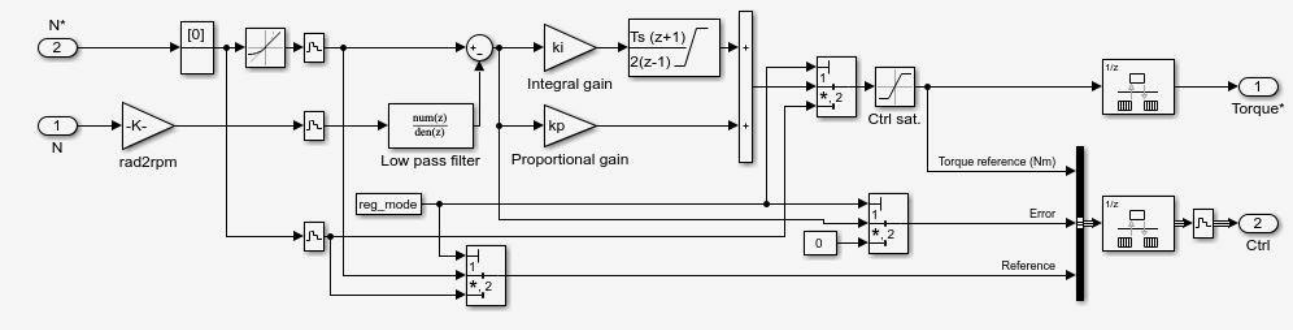

Fig. 6.5 Implementation of PI controller for Speed Control in BLDC motor

6.3 INTRODUCTION TO FUZZY LOGIC

Fuzzy logic control is an implementation of Fuzzy set theory introduced by L.A Zadeh in 1965. In the fuzzy set theory, a particular object has a degree of membership in a given set that may be anywhere in the range of 0 to 1. This property allows fuzzy logic to deal with uncertain situations in a fairly natural way . Although

fuzzy logic deals with imprecise information , it is based on sound quantitative mathematical theory .

6.3.1 OPERATING BLOCKS IN LFC

A LFC comprises of the following design steps :

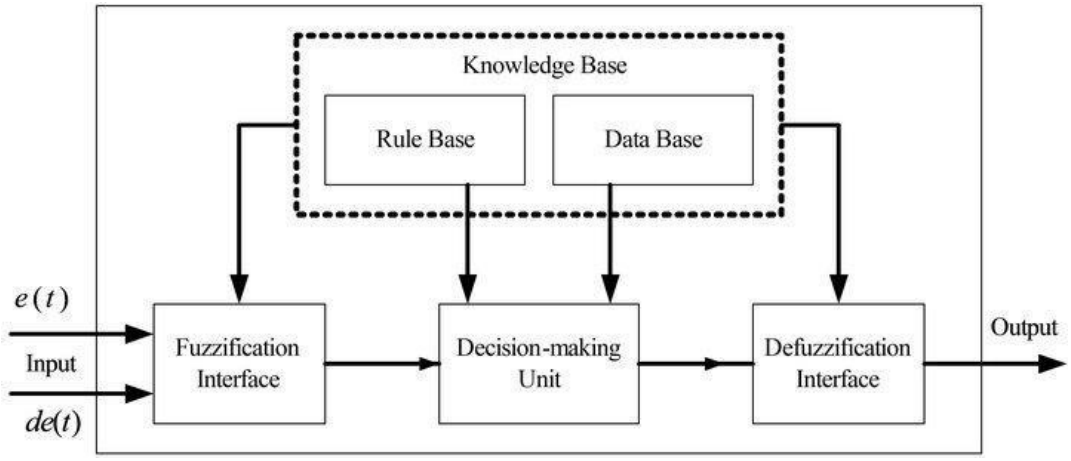

Fig. 6.6 Fuzzy Logic Block Diagram

- Define the input and control variables - determine which states of the process shall be observed and which control actions are to be considered .
- Define the condition interface - fix the way in which observations of the process are expressed as fuzzy sets.
- Design the rule base - determine which rules are to be applied under which conditions.
- Design the computational unit - supply algorithms to perform fuzzy computations. These will generally lead to fuzzy outputs.

- Determine rules according to which fuzzy control statements can be transferred into crisp control action .

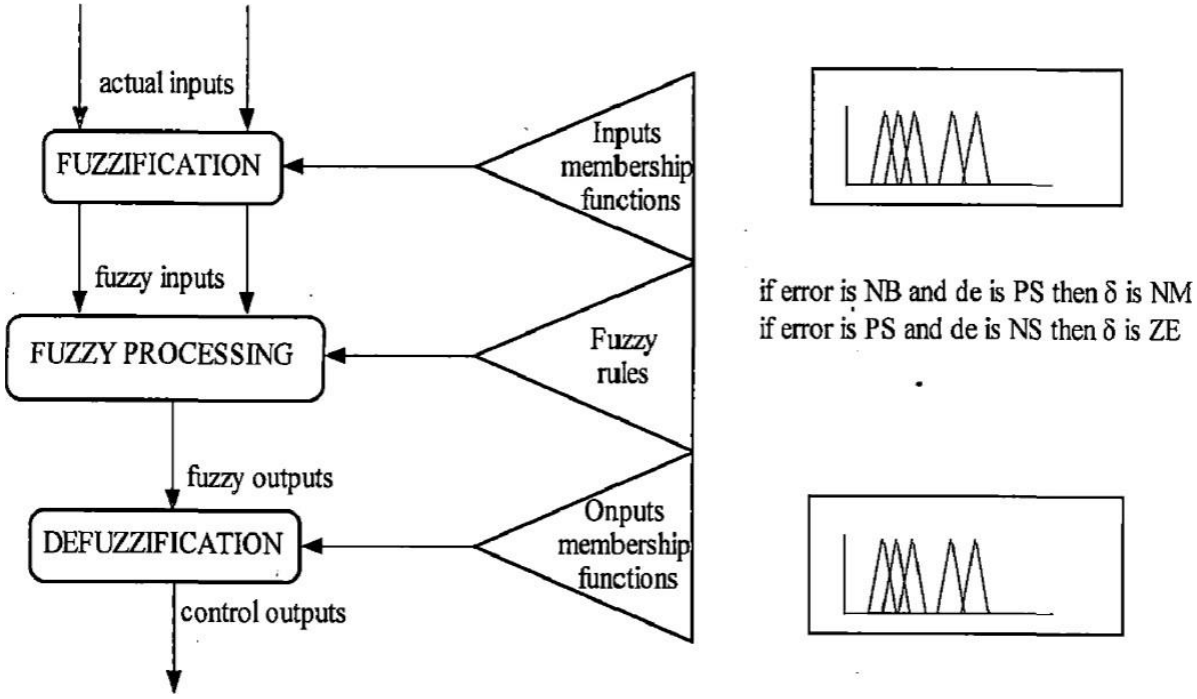

Fig. 6.7 Operation of Fuzzy Logic Controller

6.3.2 FUZZY LOGIC SETS

A fuzzy set has a graphical description that expresses how the transition from one place to another. This graphical description is called a membership function. Based upon the variable speed inputs (in rps), fuzzy variables are defined which are pictorially denoted by gradually varying triangular membership functions. The fuzzy variables are Negative Big (NB), Negative Small (NS), Zero (ZE), Positive Big (PB) and Positive Small (PS) . Membership functions can be of any shape i.e Gaussian or trapezoidal etc based upon the application . In fuzzy set terminology the possible values that speed error can assume are named as universe of discourse

and the fuzzy sets (characterised by membership functions) cover the whole universe of discourse [6] .

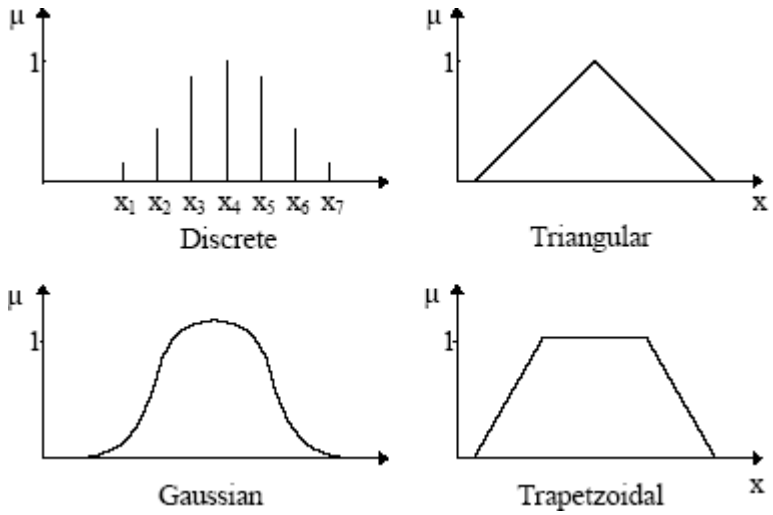

Fig. 6.8 Commonly Used Membership Functions

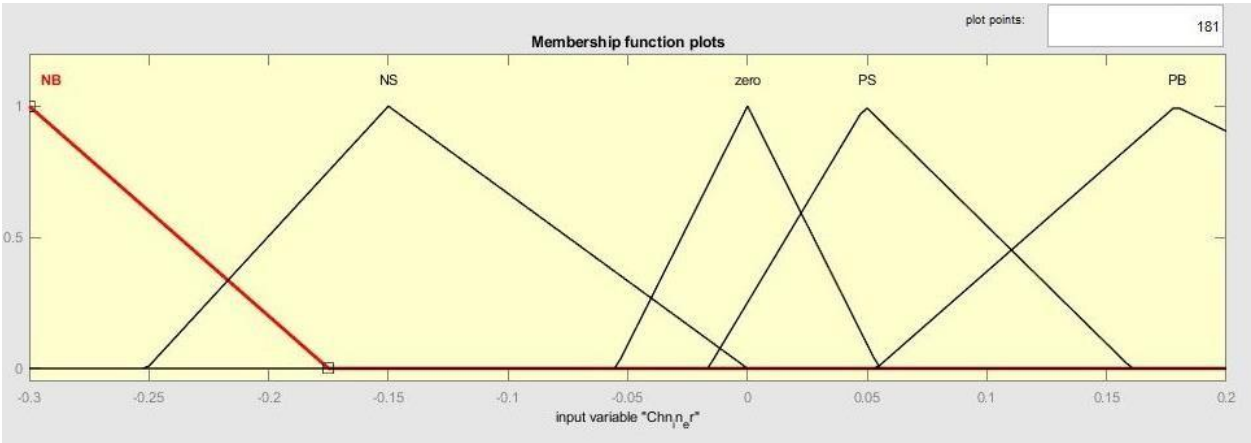

Fig. 6.9 Fuzzy sets for speed error defined using membership functions

The basic properties of Boolean algebra are valid in fuzzy set theory and are given as follows :

Union : Given two fuzzy subsets A and B of a universe of discourse X , the union A∪B is also a set of X with membership function given as

$\mu_{A\cup B}$ =max [μ_A,μ_B]

This is equivalent to Boolean OR logic .

Intersection : The intersection of two fuzzy sets A and B of the universe of discourse X , denoted by A∩B has the membership function given as

$\mu_{A\cap B}$ =min [μ_A,μ_B]

This is equivalent to Boolean AND logic .

Compliment : The complement of the given set A of the universe of discourse X , defined by $\underline{A}$, has the membership function ,

$$\mu_A(x) = 1 - \mu\underline{A}(x)$$

This is equivalent to Boolean NOT logic .

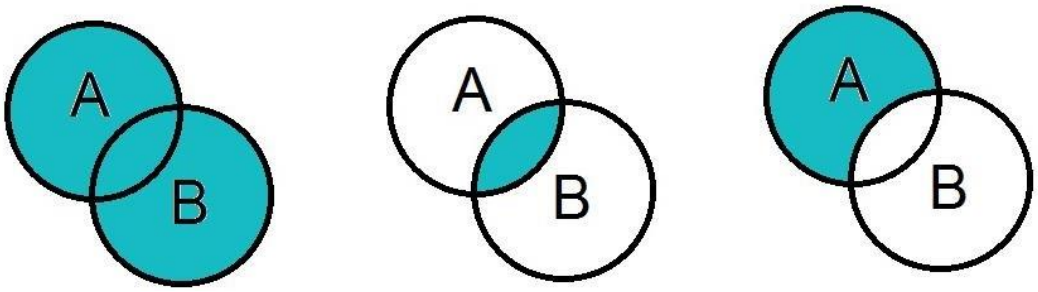

Fig. 6.10(a) Union[A∪B] , Fig. 6.10(b) Intersection [A∩B] ,

Fig. 6.10(c) Compliment $\bar{A}$

6.3.3 FUZZIFICATION

The number of fuzzy levels is not fixed and depends on the input resolution needed in an application, the larger the number of fuzzy levels, higher is the input resolution. The inputs are not quantized in the classical sense that each input is assigned to exactly one level. Instead, each input is assigned to a "membership

function " μ to each fuzzy set (i.e e and Δe) . The fuzzy controller implemented here uses triangular fuzzy-set values . Triangular functions reduce complexity in calculations .

6.3.4 FUZZY CONTROL RULES

Fuzzy control is defined by a set of IF…..THEN ..... rules(called implication) ,where the rule has the following structure :

IF i is A and B is j THEN y is C .

Where i,j,y are the fuzzy variables and A,B,C are the fuzzy sets in the universe of discourses X,Y,Z respectively .

In general a rule is n dimensional where n is the number of variables included in the rule. The individual rules are combined together to give an overall rule R which is computed by union operator as follows :

$$R = R_1 \cup R_2 \cup R_3 \ldots\ldots\ldots R_n$$

For the given rule base of the control system, the fuzzy controller determines the rules to be fired for specific input and then computes the effective control action.the composition method is one by which such control output can be generated [4] .

6.3.5 DEFUZZIFICATION

The Defuzzification goal in Mamdani-type fuzzy controllers is to produce a crisp output taking the fuzzy output obtained after the rules processing, clipping or scaling . Because the input for the defuzzification procedure is clipped membership function, the most preferred inference method is Mamdani min fuzzy Inference method . the inference result of each rule using Mamdani min fuzzy consists of two

parts , the weighting factor $w_i$of the individual rule and degree of output $C_i$according to the control table .Therefore the inferred output of each rule using Mamdani min fuzzy implication is written as

$$y_i = min\{\mu_{input(i)}, \mu_{input(j)}\}C_i$$

$$y_i = w_i C_i$$

Where $y_i$denotes the fuzzy representation of output referred by the I^{th}rule .
Since the output is a linguistic result, a defuzzification operation is performed next to obtain a crisp result . The crisp value for the final output is calculated using the centre of gravity method . The product of centroid $m_i$of C_i(obtained from control rules) and the weighing factor w_i gives the contribution of l^{th}inference results in the crisp value of the final output . The resultant output can therefore be represented as

$$\text{Final output} = \frac{\sum_{i=1}^{4} w_i}{\sum_{i=1}^{4} m_i w_i} \qquad (6.5)$$

6.4 CONTROL ALGORITHM

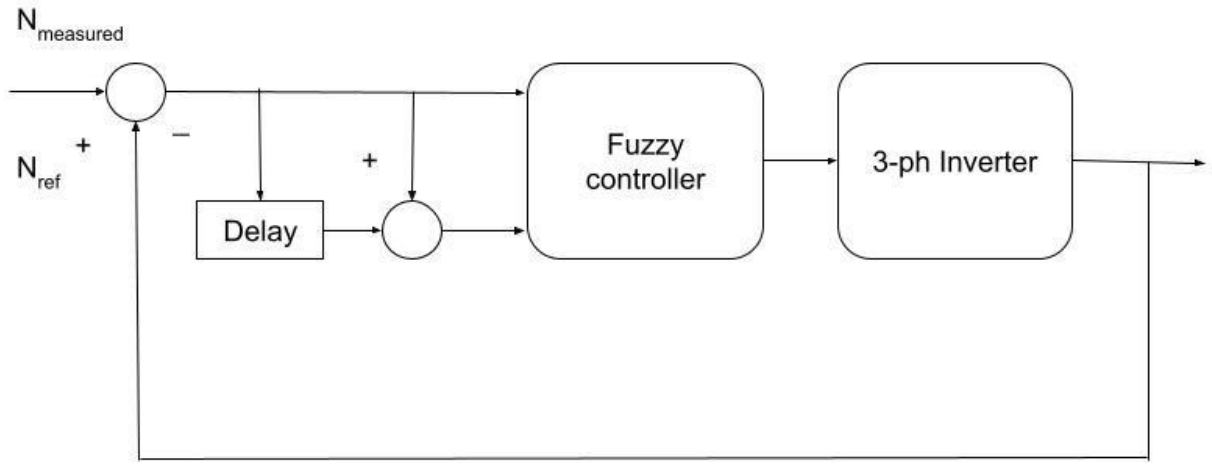

Fig. 6.11 Block diagram of Controlling Method

The basic purpose of closed loop control of a motor is to obtain smooth speed control even at dynamic load conditions . To implement this the motor speed is compared with reference speed as shown in Fig. 6.11, and this result is given as :

$$e(k) = N_{ref} - N_{measured} \quad (6.6)$$

And change in error is calculated as

$$\Delta e(k) = e(k) - e(k-1) \quad (6.7)$$

Where, N_{ref} is reference speed

$N_{measured}$ = output speed

$e(k)$ = speed error at Kthinstant

$e(k-1)$= speed error at (K-1)th instant

$\Delta e(k)$ = change in speed error at Kth instant

Therefore, the two inputs to LFC are speed error and change in speed error and according to the control law implemented, it produces the output which change input gate pulses of the 3-ph inverter . In Fig. 6.1, e denotes the error whereas $\hat{e}$ denotes the change in error .

Table 6.1

Control Rules for Fuzzy Logic

$e\ /\hat{e}$	**NB**	**NS**	**ZE**	**PS**	**PB**
NB	NB	NS	NS	NS	PB
NS	NS	NS	NS	PS	PB
ZE	ZE	NS	ZE	PB	PB
PS	NS	NS	PS	PS	PB
PB	NS	PS	PB	PS	PB

The fuzzy control rules are derived so as to reduce the ripples in torque and stator current and to stabilize the controlling speed .

- When the speed of the motor is far from the set point , the change in inverter gate pulses must be small so as to bring the output close to the set point quickly.
- When the speed of the motor is approaching the set point , a small change in inverter gate pulses is necessary .
- When the speed is approaching the set point rapidly , gate pulses must be controlled so as to prevent overshoot .
- When the set point is attained , the change in pulses must remain unchanged .

6.5 FUZZY LOGIC CONTROL BOX

There are five primary GUI tools for building, editing and observing fuzzy inference systems in the fuzzy logic toolbox. The fuzzy inference system or FIS editor Fig .6.12, the membership function editor(Fig. 6.13) , the rule editor (Fig. 6.14**)** , the rule viewer and the surface viewer .

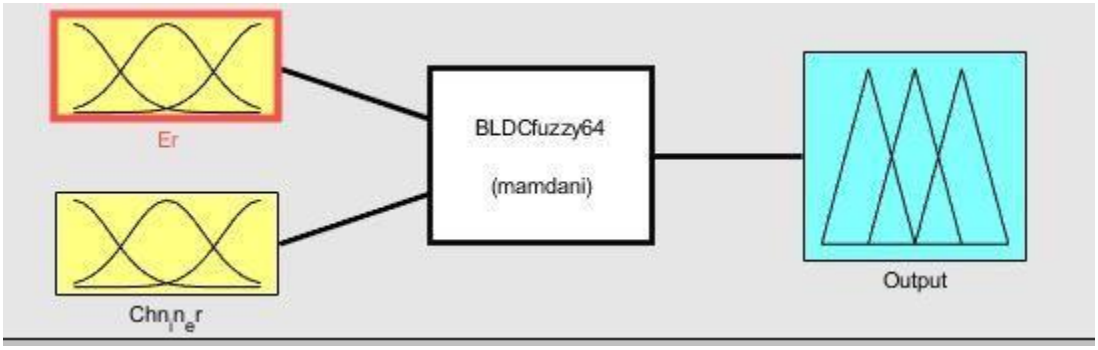

Fig. 6.12 FIS editor

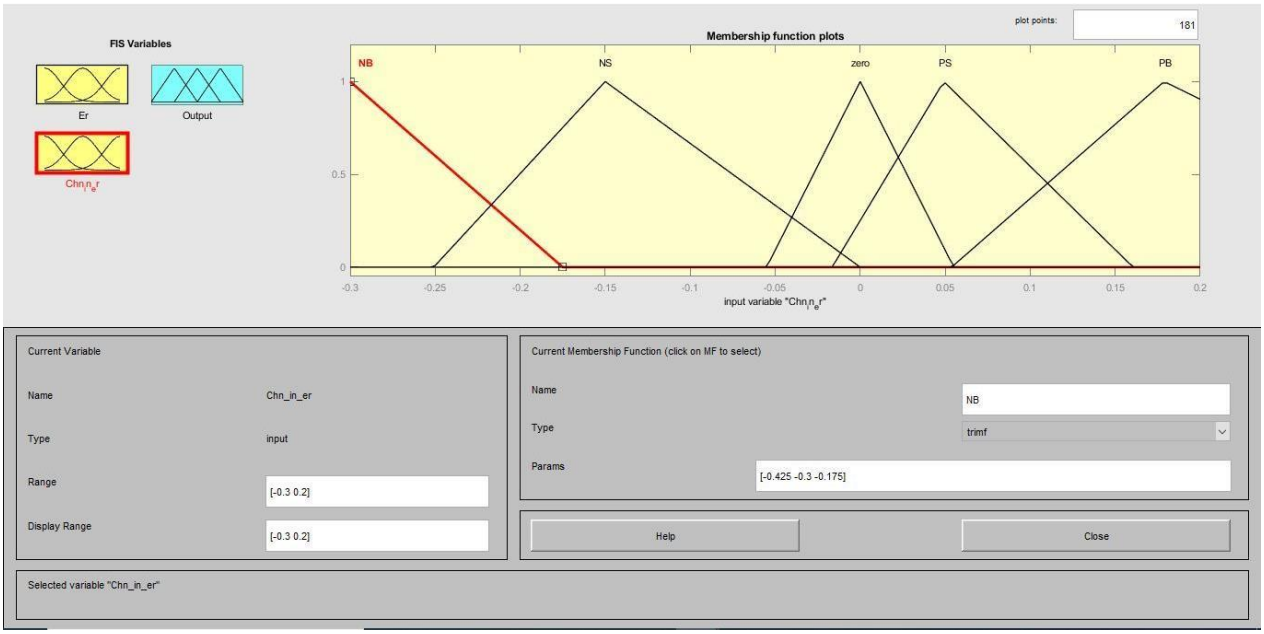

Fig. 6.13(a) Membership Function Editor for change in speed error

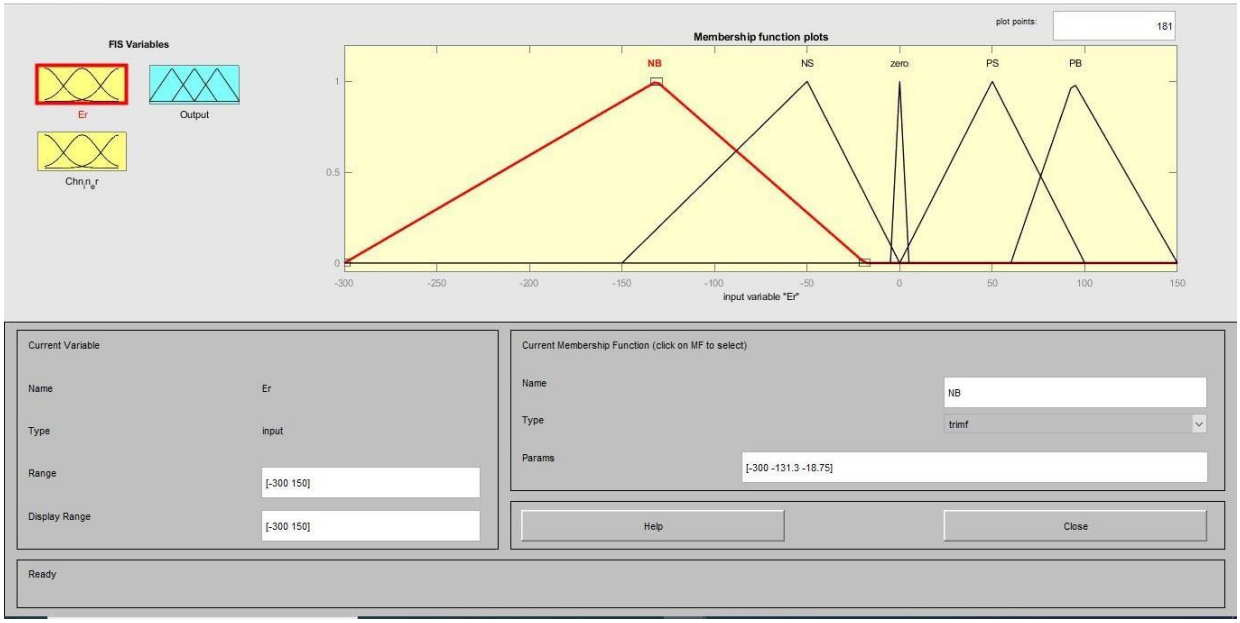

Fig. 6.13(b) Membership Function Editor for speed error

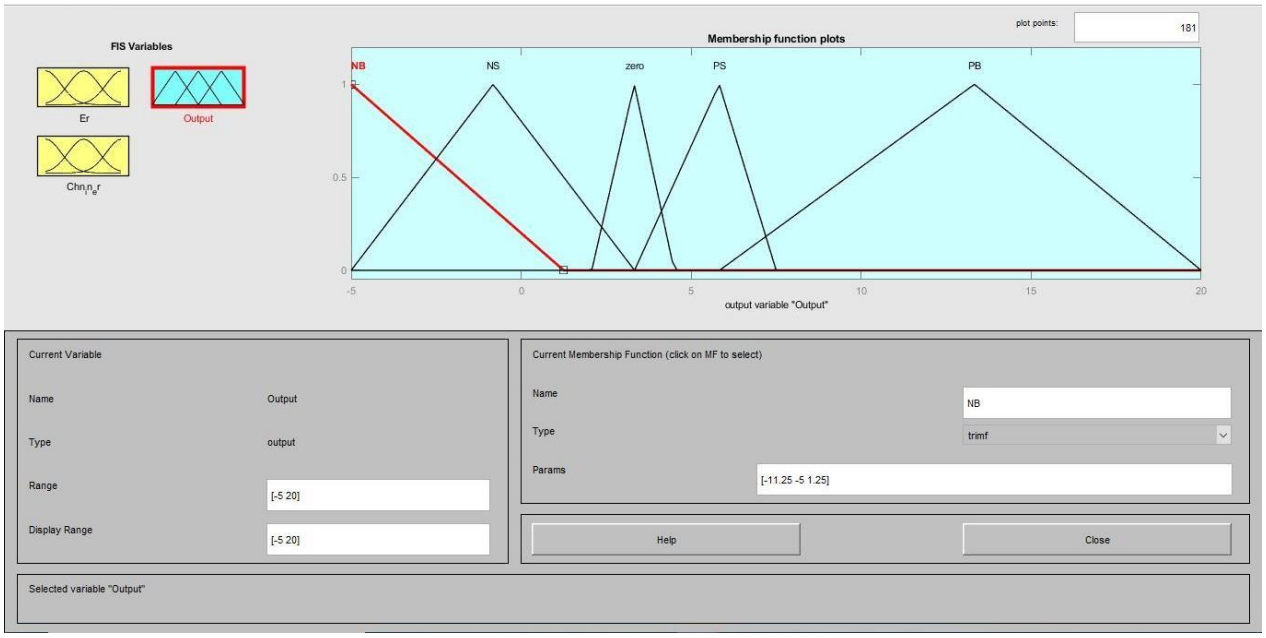

Fig. 6.13(c) Membership Function Editor for error in output

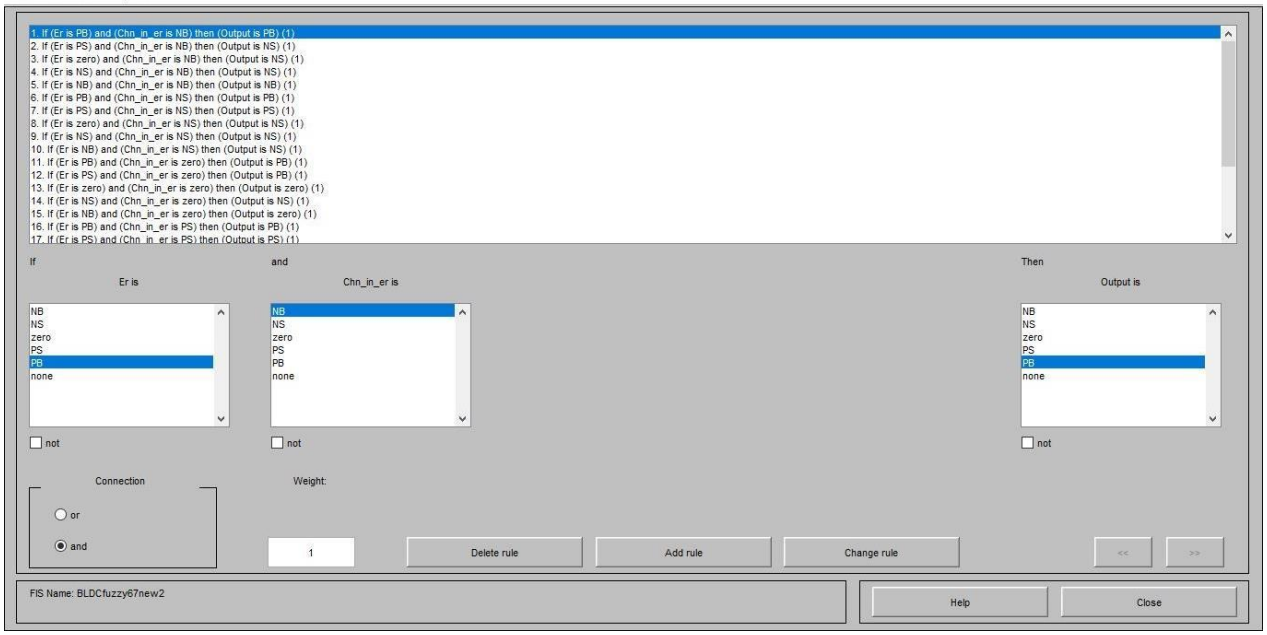

Fig. 6.14(a) Rule Editor

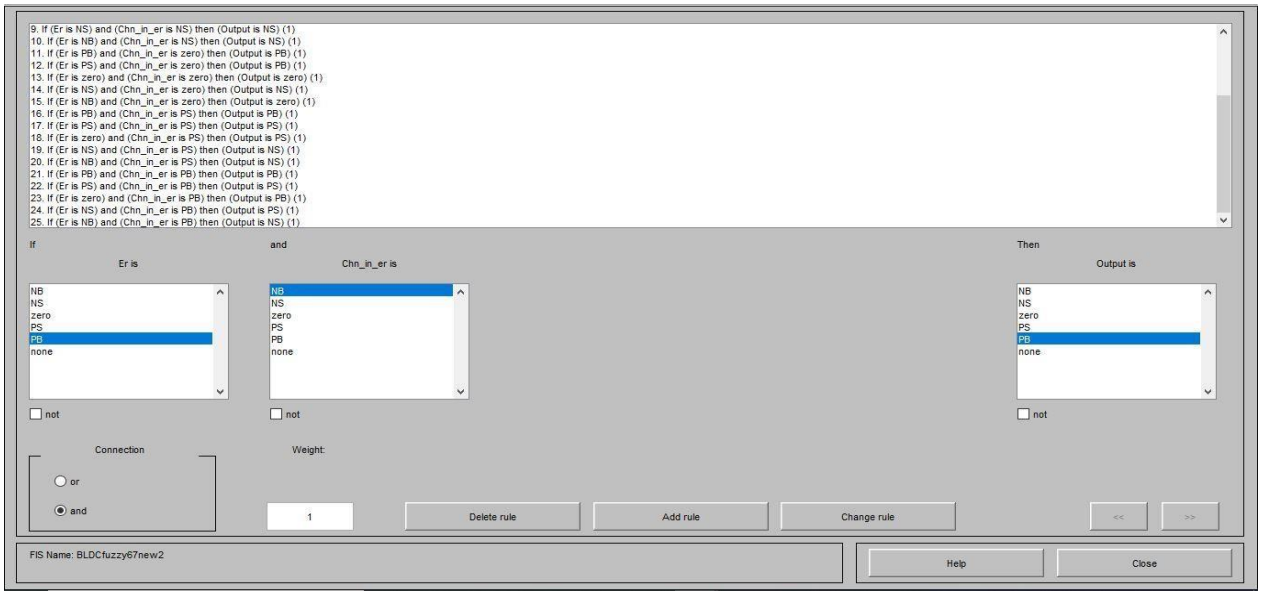

Fig. 6.14(b) Rule Editor Contd.

6.6 SIMULATION AND RESULTS

6.6.1 Introduction

Here we studied the performance of a BLDC motor . The simulation of the BLDC motor is carried out by using both PI and Fuzzy controllers . We also found out how the rotor speed, stator current and output torque varies dynamically with respect to the reference speed. This way the proposed objective of Speed regulation using a Fuzzy controller is accomplished . The simulation of the proposed system is carried out in MATLAB version R2018a using SIMULINK TOOLBOX [16] .

6.6.2 Fuzzy Controller

Figure shows the simulink model block diagram for the Fuzzy Logic Controller . Here, the two inputs namely error and change in speed error and are

properly scaled and fed to the MATLAB fuzzy logic controller [7] . The defuzzified output of Fuzzy block is scaled by scaling factors and after limiting we get the reference speed .

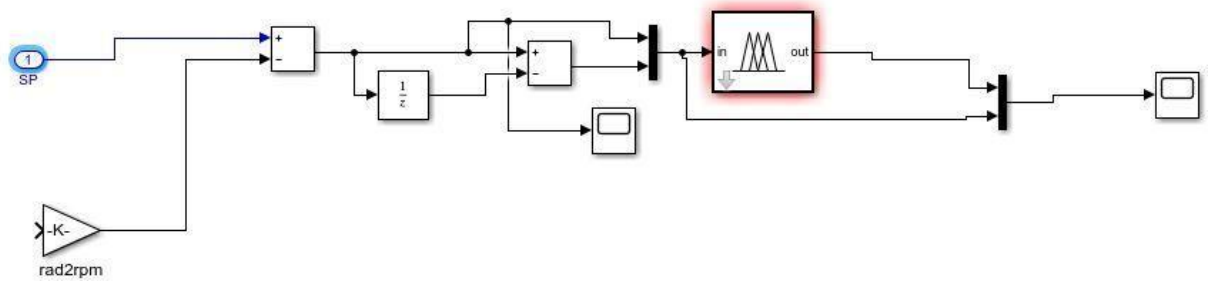

Fig. 6.15 Fuzzy Logic Controller for Speed Control in BLDC motor

6.6.3 Speed output

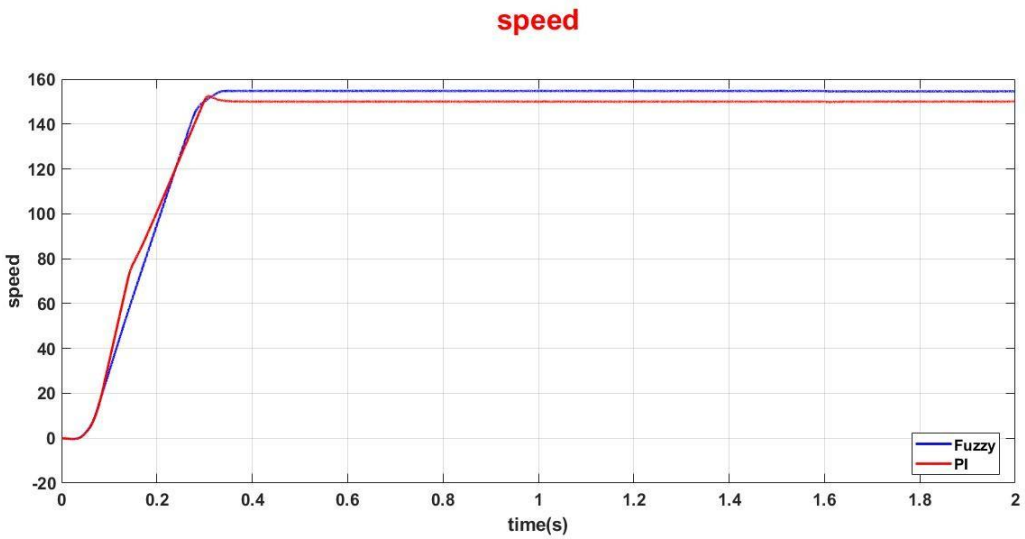

Fig. 6.16 Fuzzy Logic vs PI Controller Comparison for Speed

The above Fig. 6.16 shows the variation in speed with PI and Fuzzy controllers . Reference speed is set as 150 rad/s, based upon the simulation result from PI controller it can be observed that the actual speed reaches to

155 rad/s at t=0.37 s whereas in case of Fuzzy controller actual speed reaches 150 rad/s at t = 0.35 s .

6.6.4 Stator Current Output

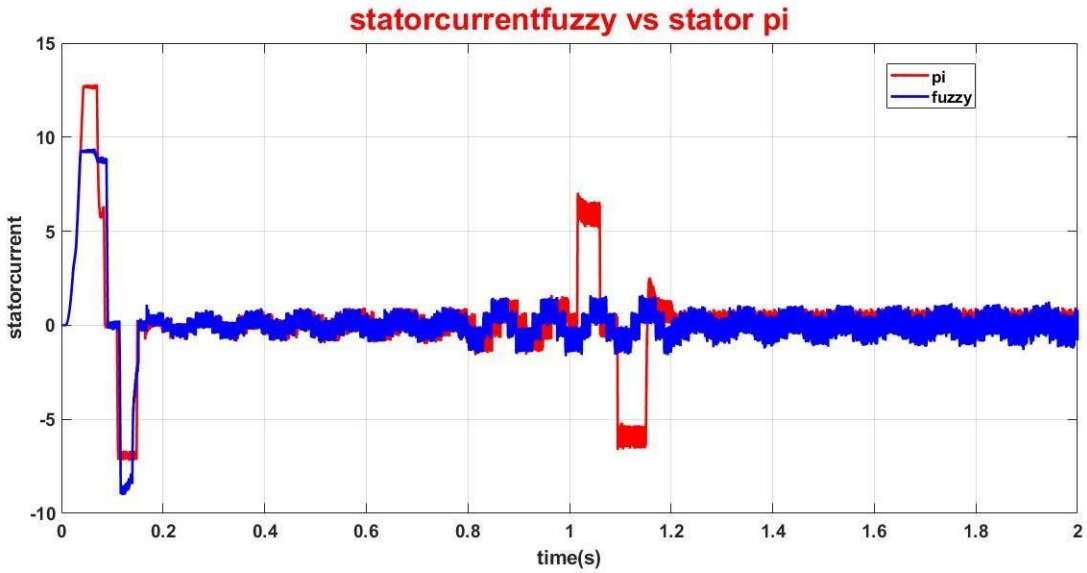

Fig. 6.17 Fuzzy Logic v PI Controller Comparison for Stator Current

The above Fig. 6.17 shows the variation in stator current with PI and Fuzzy controllers . Reference speed is set as 150 rad/s, based upon the simulation result from PI controller it can be observed that the peak current of 13 A is attained at t=0.05s and stabilizes with a few ripples after t=0.18s upto t=1s . For the same time intervals, the current using fuzzy controllers has a reduced peak value of 9.1A at t=0.04 s and stabilizes throughout the simulated time (i.e2 s) with much reduced ripples .

6.6.5 Torque Output

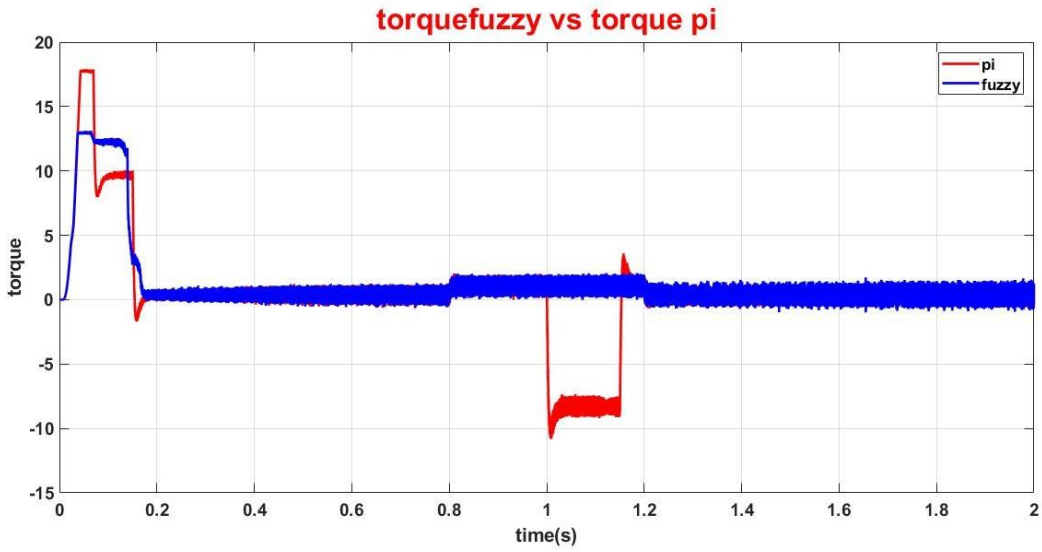

Fig.6.18 Fuzzy Logic v PI Controller Comparison for Torque

The above Fig. 6.18 shows the variation in torque with PI and Fuzzy controller . Reference speed is set as 150 rad/s, based upon the simulation result from PI controller it can be observed that the peak torque of 17 Nm is attained at t=0.05s and stabilizes with a few ripples after t=0.18s upto t=1s . For the same time intervals, the torque using fuzzy controller has a reduced peak value of 13 Nm at t=0.04 s and stabilizes throughout the simulated time (i.e 2 s) with much reduced ripples and under-shoots .

6.7 RESULTS AND DISCUSSION

In this chapter a detailed MATLAB analysis on the effects of various controllers over the system is simulated and its results are compared to arrive at best solutions. The principle of operation, working on various controllers and its advantages and disadvantages are studied. The tuning method of the controller is also discussed and practically carried out to match our requirements.

Graphical representations are also presented to arrive at a better understanding. The MATLAB model of the control strategy used to produce the inverter gate pulses to enable smooth speed control of the motor has been presented . In addition to this , the optimization of the power flow cycle between two sources using bidirectional convertors is also presented . The mathematical analysis done aids in producing efficient results along with MATLAB analysis.

We have observed that when the motor speed attains its steady state value of 150 rad/s , the current and the torque oscillate near zero . This oscillation is comparatively reduced when a FLC is used in place of a PI controller . The low values for torque and current (i.e close to 0) at the desired speed is liable to the minimal rated motor current of 4 A only. The peak overshoot and the peak under-shoot encountered using the PI controller diminish gradually with time . FLC assists in attainment of steady state and removal of steady-state error e_s.

CHAPTER 7

CONCLUSION

A Fuel Cell Electric Vehicle is a topology of electric vehicles that is designed and engineered to operate on fuel cells . In this proposed work , a DC-DC converter is employed to produce a constant DC link voltage to propel the BLDC motor. The initial objective of this work is to ensure an uninterrupted and a constant power supply to drive the tractive system. A Bidirectional converter commands the power flow between the source and the load as well as between the two sources used i.e Fuel Cell and Li-ion Battery . The complete control system has been developed, analysed, and validated by simulation study. Performances have then been evaluated in detail for different operating conditions. All the simulation results proposed in this work is done using MATLAB/Simulink.

In the future scope of work , the proposed speed control mechanism would be upgraded with the help of Artificial Neural Networks (ANN) to get immaculate results. In addition to this, Model Predictive Control (MPC) algorithm can be applied in order to reduce the system complexity and increase the speed of operation of the control system .

REFERENCES

[1]. Deepak Ravi, BandiMallikarjuna Reddy, Shimi S.L., Paulson Samuel (2018) . Bidirectional dc to dc Converters: An Overview of Various Topologies, Switching Schemes and Control Techniques International Journal of Engineering &Technology .doi :10.14419/ijet.v7i4.5.20107

[2]. Ural Bayrak, Zehra&Gençoğlu, M.T.. (2010). Mathematical Models of PEM Fuel Cells. Proc. 5th Int. Ege Energy Symp. Exhib.

[3]. Mu, Dazhong& Jiang, Jiuchun& Zhang, Caiping. (2013). Online Semiparametric Identification of Lithium-Ion Batteries Using the Wavelet-Based Partially Linear Battery Model. Energies 6. 2583-2604. doi:10.3390/en6052583.

[4]. Bai, Ying & Wang, Dali. (2007). Fundamentals of Fuzzy Logic Control — Fuzzy Sets, Fuzzy Rules and Defuzzification. doi:10.1007/978-1-84628-469-4_2.

[5]. Obulesh, Y &Ch, Sai Babu & Rao, A.. (2012).” Mathematical modeling of bldc motor with closed loop speed control using pid controller under various loading conditions.” ARPN Journal of Engineering and Applied Sciences. 7. 1321-1328.

[6]. http://shodhbhagirathi.iitr.ac.in:8081/jspui/image/pdf/web/viewer. Html ?file=/jspui/bitstream/123456789/11320/1/EEDG14488.pdf

[7]. Faddel, Samy& Mohamed, Ahmed & Mohammed, Osama. (2017). "Fuzzy logic-based autonomous controller for electric vehicles charging under different conditions in residential distribution systems. Electric Power Systems Research." 148.48-58. doi:10.1016/j.epsr.2017.03.009.

[8]. https://www.mathworks.com/help/phys mod/sps/ug/ac7-brushles s-dc-motor-drive-during-speed-regulation.html;jsessionid=db5a837e8c 579a957fe7 65a28 c69

[9]. Iftikhar, Muhammad & Aamir, Muhammad & Waqar, Asad&Naila, & Muslim, Fahad &Alam, Imtiaz. (2018)." Line-Interactive Transformerless Uninterruptible Power Supply (UPS) with a Fuel Cell as the Primary Source. "Energies. 11. 542. doi:10.3390/en11030542.

[10]. https://letstalkscience.ca/educational-resources/stem-in-context/how-Does-a-lithium-ion-battery-work

[11]. X. Zhou et al., "The current research on electric vehicle," (2016) Chinese Control and Decision Conference (CCDC), Yinchuan, China, 2016, pp. 5190-5194, doi: 10.1109/CCDC.2016.7531925.

[12]. S. Chander, P. Agarwal and I. Gupta, "Design, modeling and simulation of DC-DC converter," 2010 Conference Proceedings IPEC, Singapore, 2010, pp. 456-461, doi: 10.1109/IPECON.2010.5697039.

[13]. Uddin, K.; Picarelli, A.; Lyness, C.; Taylor, N.; Marco, J. "An Acausal Li-Ion Battery Pack Model for Automotive Applications. "*Energies* **2014**, *7*, 5675-5700. https://doi.org/10.3390/en7095675

[14]. A. Platon, S. Oprea, A. Florescu and S. G. Rosu, "Simple and Digital Implementation of PI Controller Used in Voltage-Mode Control," 2018 10th International Conference on Electronics, Computers and Artificial Intelligence (ECAI), Iasi, Romania, 2018, pp. 1-6, doi: 10.1109/ECAI.2018.8679078.

[15]. M. Amirabadi and S. Farhangi, "Fuzzy Control of a Hybrid Power Source for Fuel Cell Electric Vehicle using Regenerative Braking Ultracapacitor," 2006 12th International Power Electronics and Motion Control Conference, Portoroz, Slovenia, 2006, pp. 1389-1394, doi: 10.1109/EPEPEMC.2006.4778597.

[16]. Kayaalp, İlker&Demirdelen, Tuğçe&Tümay, Mehmet. (2016). "A Novel Fuzzy Logic Control for Bidirectional DC-DC Converter and Comparison with Dual Phase-Shift Control Method in Medium Voltage Applications." doi:10.1109/CIVEMSA.2016.7524324.

[17]. El Brogy, Walaa&Fkirin, M. A. &Moustafa Hassan, Mohamed. (2013). Speed Control of DC Motor Using PID Controller Based on Artificial Intelligence Techniques. 196-201.

[18]. Treffinger, Peter & Brinner, Andreas &Schöll, Roland & Friedrich, Horst. (2006). Fuel Cell and Hydrogen Vehicles - State of the Art and Challenges for improved Materials.

[19]. https://www.mpoweruk.com/hydrogen_fuel.htm

[20]. K. Bhatt, R. A. Gupta and N. Gupta, "Comparative Analysis and Control of Bidirectional DC-DC Converters," 2019 IEEE 1st International Conference on Energy, Systems and Information Processing (ICESIP), Chennai, India, 2019, pp. 1-6, doi: 10.1109/ICESIP46348.2019.8938349.

[21]. Haiping Xu, Gang Ma, Changfu Sun, Xuhui Wen and Li Kong, "Implementation of a bi-directional DC-DC converter in FCEV," Sixth International Conference on Electrical Machines and Systems, 2003. ICEMS 2003., Beijing, China, 2003, pp. 375-378 vol.1.

[22]. Kim, Taehyung & Yang, Jingan. (2009).” Control of a brushless DC motor/generator in a fuel cell hybrid electric vehicle.” 1973 - 1977. doi: 10.1109/ISIE.2009.5215662.

[23]. Mu, D.; Jiang, J.; Zhang, C. “Online Semiparametric Identification of Lithium-Ion Batteries Using the Wavelet-Based Partially Linear Battery Model.” *Energies* **2013**, *6*, 2583-2604. https://doi.org/10.3390/en6052583 .

[24]. Rao, L. & Gairola,S. (2016). A comparative study of Bidirectional DC-DC converter & its interfacing with two battery storage systems. 1-6. doi:10.1109/ICPEICES.2016.7853175.